Atmos. Chem. Phys., 13, 9543–9564, 2013
www.atmos-chem-phys.net/13/9543/2013/
doi:10.5194/acp-13-9543-2013


Atmospheric Chemistry and Physics Open Access

# The diurnal and semidiurnal tides over Ascension Island (8° S, 14° W) and their interaction with the stratospheric quasi-biennial oscillation: studies with meteor radar, eCMAM and WACCM

**R. N. Davis[1], J. Du[2], A. K. Smith[3], W. E. Ward[4], and N. J. Mitchell[1]**

[1]Centre for Space, Atmospheric and Oceanic Science, Department of Electronic and Electrical Engineering, University of Bath, BA2 7AY, UK
[2]Department of Physics and Astronomy, University of Louisville, KY 40292, USA
[3]Atmospheric Chemistry Division, National Center for Atmospheric Research, Boulder, CO, USA
[4]Department of Physics, University of New Brunswick, Fredericton, NB EB3 5A3, Canada

*Correspondence to:* R. N. Davis (rnd24@bath.ac.uk)

Received: 15 December 2012 – Published in Atmos. Chem. Phys. Discuss.: 19 February 2013
Revised: 9 August 2013 – Accepted: 12 August 2013 – Published: 27 September 2013

**Abstract.** Horizontal winds in the mesosphere have been measured over Ascension Island (8° S, 14° W) in the tropical mid-Atlantic region throughout the years 2002–2011. The observations were made by a very high frequency (VHF) meteor radar. The observations reveal the presence of atmospheric tides of large amplitude. The observations are analysed to characterise the seasonal and interannual variability of the diurnal and semidiurnal tides. Monthly-mean diurnal tidal amplitudes are found to reach values as large as 48 m s$^{-1}$ in the meridional component and 41 m s$^{-1}$ in the zonal. A semiannual seasonal variation is found in diurnal tidal amplitudes with amplitude maxima at the equinoxes and amplitude minima at the solstices. Diurnal tidal meridional vertical wavelengths are generally in the range 24–30 km. The diurnal zonal vertical wavelengths are similar to the meridional, except for the winter months when the zonal vertical wavelengths are much longer, occasionally exceeding 100 km. Semidiurnal amplitudes are observed to be significantly smaller than diurnal amplitudes. Semidiurnal vertical wavelengths range from 20 to more than 100 km. Our observations of tidal amplitudes and phases are compared with the predictions of the extended Canadian Middle Atmosphere Model (eCMAM) and the Whole Atmosphere Community Climate Model (WACCM). Both eCMAM and WACCM reproduce the trend for greater diurnal amplitudes in the meridional component than the zonal. However, eCMAM tends to overestimate meridional amplitudes, while WACCM underestimates both zonal and meridional amplitudes. Vertical wavelength predictions are generally good for both models; however, eCMAM predicts shorter diurnal zonal vertical wavelengths than are observed in winter, while WACCM predicts longer zonal vertical wavelengths than observed for the semidiurnal tide for most months. Semidiurnal amplitude predictions are generally good for both models. It is found that larger-than-average diurnal and semidiurnal tidal amplitudes occur when the stratospheric quasi-biennial oscillation (QBO) at 10 hPa is eastwards, and smaller-than-average amplitudes occur when it is westwards. Correlations between the amplitude perturbations and the El Niño Southern Oscillation are also found. The precise mechanism for these correlations remains unclear.

## 1 Introduction

The mesosphere and lower thermosphere (MLT) are host to a wide range of oscillations including tides, planetary waves and gravity waves that can manifest in the wind, temperature and pressure fields. However, at most latitudes the dominant oscillations are the tides, which can reach amplitudes of many tens of metres per second.

The migrating (sun-synchronous) tides are excited primarily by the diurnal cycle in solar heating of gases in the atmosphere. These gases include water vapour, which absorbs

infra-red radiation in the troposphere and ozone in the stratosphere/mesosphere, which absorbs ultra-violet radiation. The release of latent heat in deep tropospheric convection at tropical latitudes also contributes to the excitation of these tides (e.g. Hagan and Forbes, 2003). There also exist non-migrating (non-sun-synchronous) tides. These non-migrating tides can be excited by a number of mechanisms, including longitudinal differences in tropospheric radiative heating and tropospheric latent heat release (e.g. Williams and Avery, 1996; Hagan and Forbes, 2003; Zhang et al., 2010) and non-linear interaction between migrating tidal modes and planetary waves (e.g. Oberheide et al., 2002).

Observations have revealed the largest amplitude tidal modes to have periods of 24, 12 and 8 h. These are the diurnal, semidiurnal and terdiurnal tides. At tropical latitudes, the diurnal tide tends to dominate. At middle and high latitudes, the semidiurnal tide tends to dominate. The terdiurnal tide generally reaches smaller amplitudes, but can nevertheless be significant (e.g. Teitelbaum et al., 1989; Younger et al., 2002; Du and Ward, 2010).

Atmospheric tides play an important role in the coupling and dynamics of the atmosphere. In particular, the tides transport momentum and can deposit it at heights above the tidal source region, thus contributing to the wave-driving of the middle atmosphere (e.g. Miyahara et al., 1993; Lieberman and Hays, 1994). The wind and temperature perturbations of tides can act to filter the field of ascending gravity waves and so modulate gravity-wave fluxes of energy and momentum (e.g. Fritts and Vincent, 1987; Beldon and Mitchell, 2010). Non-linear interactions between tides and planetary waves can generate planetary-scale secondary waves which are thought to play a key role in tidal variability and impose a modulation on tidal amplitudes at planetary-wave periods (e.g. Beard et al., 1999; Chang et al., 2011; Forbes and Moudden, 2012). Additionally, short-term tidal variability may result from the refractive effects of planetary waves (e.g. Riggin et al., 2003). Tides are believed to be an important source of variability of polar mesospheric clouds, where the tidal perturbations of temperature influence the ice crystal population of the clouds (e.g. Chu et al., 2001; Fiedler et al., 2005). Tides are also believed to be important agents in the coupling of the atmosphere and the ionosphere (e.g. Immel et al., 2006; Pedatella et al., 2012).

However, despite the recognised importance of tides, many uncertainties remain about their excitation, interaction with other tides and waves, their variability on timescales from a few days to the interannual and their role in coupling the middle and upper atmosphere. Advances in general circulation models (GCMs) have allowed tides in the MLT to be represented, but significant differences often remain between the predictions of GCMs and observations. A critical task, therefore, is to use observations of tides to constrain their representation in GCMs. Ground-based meteor and medium-frequency (MF) radars are well suited to observations of tides in the MLT. In particular, the radars offer excellent time resolution of the order of a few hours and so can investigate tidal variability on short timescales. The radars are able to operate for extended intervals and so can also investigate the seasonal and interannual variability of tides. These observations provide a powerful complimentary technique to satellite observations which can investigate zonal wavenumbers, but lack the good time resolution offered by the ground-based measurements. In this study we will exploit the capabilities of radars to make extended measurements to investigate the tides of the tropical mesosphere.

Tides in the MLT region have been reasonably well characterised at the high and middle latitudes (e.g. Manson et al., 1988, 1989, 2009; Vincent et al., 1988; Avery et al., 1989; Portnyagin et al., 1993; Fraser et al., 1995; Mitchell et al., 2002). At these latitudes the diurnal tidal modes are predominantly trapped, and so in the MLT region the semidiurnal tide has larger amplitudes.

However, classical tidal theory predicts that diurnal modes are free to propagate upwards at latitudes equatorwards of $\sim 30°$ (e.g. Lindzen, 1967; Lindzen and Chapman, 1969). We would thus expect the tropical MLT to be dominated by large-amplitude diurnal tides.

In contrast to the situation at middle and high latitudes, there have been relatively few radar studies in the tropical regions. Kumar et al. (2008) reported results from 1 yr of meteor radar observations at Trivandrum (8.5° N, 77° E). They focused on short-term variability and used bispectral analysis to find evidence of tidal–planetary-wave interactions. Sridharan et al. (2010) investigated 15 yr of MF radar winds and tides at Tirunelveli (9° N, 78° E) and examined correlations with the solar cycle, quasi-biennial oscillation (QBO) and the El Niño Southern Oscillation (ENSO). Chang and Avery (1997) reported the results from 5 yr of meteor radar observations made at Christmas Island (2° N, 158° W). Buriti et al. (2008) reported results from 1 yr of meteor radar observations made at Cariri (7.4° S, 36.5° W). The results from this location are particularly interesting because it is at a similar latitude to Ascension Island but displaced by approximately 22° westwards.

Tsuda et al. (1999) compared diurnal tide radar results between three equatorial sites and found good agreement between Jakarta (6° S, 107° E) and Pontianak (0° N, 109° W) but significant discrepancies with Christmas Island (2° N, 158° W). Friedman et al. (2009) compared the semidiurnal components at Arecibo (18° N, 67° W) and Maui (21° N, 186° W) as measured by lidar with the satellite results from SABER and found that local effects create amplitude perturbations that were missed by SABER's temporal averaging and geographic sampling.

A number of studies have reported strong interannual variability of tidal amplitudes (e.g. Fritts and Isler, 1994; Burrage et al., 1995; Vincent et al., 1998). Some of these studies have suggested that the stratospheric QBO acts to modulate tidal amplitudes in the MLT region. For example, Vincent et al. (1998) compared observations made by radar at Adelaide

(35° S, 138° E), Kauai (22° N, 160° W) and Christmas Island (2° N, 158° W) and found strong evidence that higher diurnal tidal amplitudes occur over Adelaide when the QBO is in its eastwards phase. However, the correlation at the other sites was less convincing, possibly as a result of the shorter datasets made at those sites. Gurubaran et al. (2009) similarly found no trace of QBO signatures in tidal amplitudes over Kauai, but found strong QBO signals in tidal amplitudes over Tirunelveli (8.7° N, 77.8° E). Xu et al. (2009a) used SABER observations of the diurnal tide to suggest that its amplitudes are modulated by the QBO. Wu et al. (2011) considered TIDI observations and reported that the semidiurnal response to the QBO was much smaller than the response of the diurnal tide.

Modelling studies of tides have made considerable progress in recent years, and a number of studies have compared observations with model results (e.g. Burrage et al., 1995; Fraser et al., 1995; Chang and Avery, 1997; Mitchell et al., 2002; Andrioli et al., 2009; Manson et al., 1999).

Note that at any one point on the Earth the observed tides will be a superposition of various migrating and non-migrating modes, perhaps resulting in significant longitudinal variability. To obtain realistic predictions of tidal amplitudes and phases for a single site, models must therefore reproduce the major migrating and non-migrating tidal components. Comparisons with single-site observations are thus a demanding but very useful test of the representations of tides in models and essential to guide future model development (e.g. Ward et al., 2010).

This paper presents results from a meteor radar deployed on Ascension Island (8° S, 14° W) in the tropical mid-Atlantic sector. Here we report observations of the diurnal and semidiurnal tides in the zonal and meridional winds at heights between 80 and 100 km. These results are compared with the predictions of the extended Canadian Middle Atmosphere Model (eCMAM) and Whole Atmosphere Community Climate Model (WACCM). The radar began operating in 2001, and so the extended dataset available is particularly suitable for investigating the relationship between tides and the QBO in stratospheric zonal winds.

Section 2 describes the data used and the analysis methods. Section 3 presents the results obtained. Section 4 offers a discussion of the results and comparisons with other studies, and a summary is given in Sect. 5.

## 2 Data and analysis

The wind data used in this study were obtained by a commercially produced SKiYMET VHF (very high frequency) radar located on Ascension Island (7.9° S, 14.4° W). The radar operates in an all-sky configuration. The radio frequency used is 43.5 MHz. Radial velocity measurements inferred from the Doppler shift of wind-blown meteor-trail echoes are used to derive hourly-mean zonal and meridional winds. The wind measurements are binned into six height gates centred at 80.5, 84.5, 87.5, 90.5, 93.5 and 97.0 km, respectively. The radar began operating in May 2001, and all available data were used in this study.

Ascension Island's tropical location results in a strong diurnal cycle in meteor count rates. As an example, the average hourly-meteor count rate considering all meteors recorded in 2005 is shown in Fig. 1a. From the figure, it can be seen that the number counted at 06:00 LT outnumbers the count rate at 18:00 LT by approximately a factor of ten. The vertical distribution of these meteors is shown in Fig. 1b. The figure shows that the greater majority of meteors are collected at heights between 80 km and 100 km and that the distribution peaks at a height of around 90 km. An example of the distribution of meteor detections as a function of azimuth and horizontal range is presented in Fig. 1c. The figure shows that the great majority of meteor detections occur within a collecting volume which is approximately circular and of diameter $\sim$ 300 km. The white circular gaps are due to the radar receivers being briefly short-circuited to prevent saturation by the direct wave during the transmission of successive pulses. Meteors thus can not be detected at these narrow ranges. The distributions of meteors presented in Fig. 1 are similar to those that would be observed at middle and high latitudes except for the larger ratio in the tropics of maximum to minimum meteor counts over the diurnal cycle.

The hourly horizontal winds recorded by the radar were used to determine tidal parameters. For this investigation, a linear least-squares fit was performed which returned the amplitudes and phases of the diurnal, semidiurnal, terdiurnal and quarter-diurnal tides along with the magnitude of the background wind. This was applied to the zonal and meridional winds recorded by the radar. The fits were applied to windows of four-day length, stepped in one-day increments through the time series of zonal and meridional winds (e.g. Mitchell et al., 2002; Kumar et al., 2008). Each height gate was treated separately and a requirement made that results were only recorded if data were present for more than 70 % of the hours within each 4-day window.

The monthly-mean amplitudes and phases of each tidal component within a given month were then calculated by using vector averaging. Note that this method generally produces slightly smaller monthly means than a geometric average because of fluctuations in tidal phase. The results of this analysis are time series of monthly-mean tidal amplitudes and phases in six independent height gates and in zonal and meridional components for the diurnal and semidiurnal tides from October 2001 to June 2011 – albeit with some gaps.

Ascension Island is a demanding environment in which to operate, and so the radar has not operated in a continuous manner since deployment. Figure 2 presents a schematic diagram illustrating the intervals of time during which the radar was operational from 2001 to 2011. Some height gates may have detected sufficient meteors for winds to be calculated while others recorded too few. There are two large gaps in

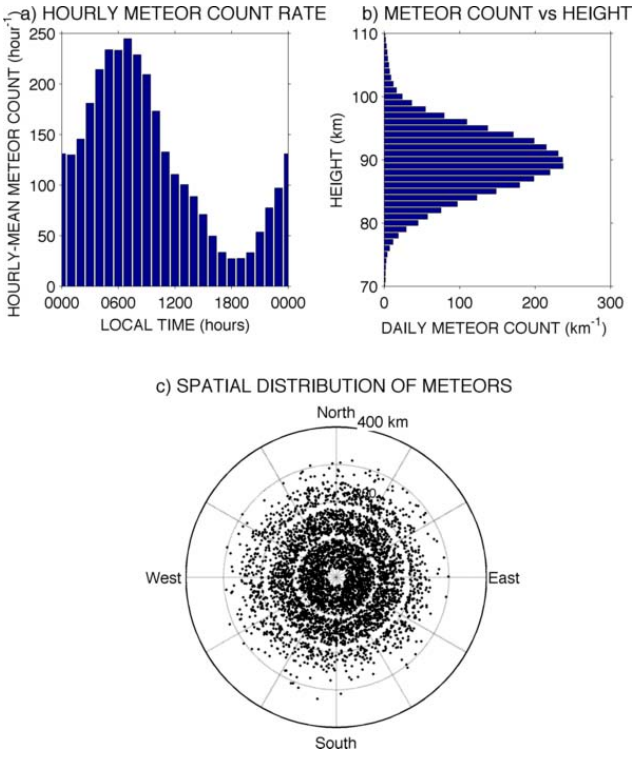


**Fig. 1. (a)** The diurnal cycle of meteor counts detected by the Ascension Island meteor radar (calculated from the ∼ 200 000 meteors detected in 2005). **(b)** The vertical profile of these meteor counts as a function of height, presented as meteor counts per km. **(c)** The distribution of meteors detected on 22 July 2005 projected onto a horizontal plane.

the data, from October 2003 to May 2004 and May 2007 to March 2009, caused by the radar being off-air for an extended time.

In this study we will make use of two models: eCMAM and WACCM. The extended CMAM, or eCMAM (Fomichev et al., 2002; Du et al., 2007), extends from the surface to heights of about 210 km. The governing equations are solved in spectral space with triangular truncations at wavenumber 32 (T32), which corresponds to a horizontal grid of approximately $6.0° \times 6.0°$ near the Equator. The vertical resolution varies from 150 m near the surface to 2 km near the tropopause and 3 km in the regions further above. The geometric heights are calculated from globally averaged geopotential heights and so are approximations with deviations of up to 5 km possible. Tidal oscillations are self-consistently generated from short- and long-wave radiation absorption, large-scale condensation and convective heating. Non-orographic gravity waves are parameterized using the Doppler-spread parameterization of Hines (1997a, b).

The third-year data from a four-year run of the eCMAM are used here. The model sampling time interval was 3 h. The model output was first converted to time series of complex amplitude for a given wavenumber at each latitude and height

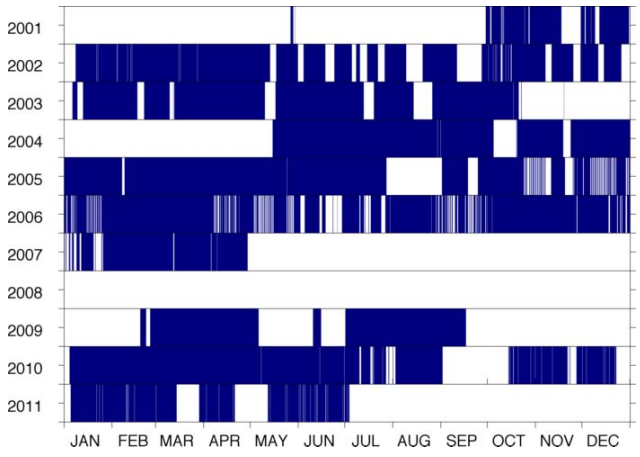


**Fig. 2.** Schematic diagram showing when the Ascension Island radar has been operational (blue) and non-operational (white) since deployment in 2001.

by summing over the spherical harmonics associated with wavenumber. These time series were then Fourier analysed in time to produce the frequencies at a particular wavenumber. The modelled horizontal winds were analysed to delineate the tides for zonal wavenumber −5 to +5. The tidal results presented here are from the closest grid point to Ascension Island, which is 10° W, 8° S. The data window used was 4 days long, advanced in 2-day increments. The monthly-mean amplitudes and phases of each tide were calculated by using vector averaging in the same manner as the radar analysis. Refer to Du et al. (2007) for more details on this data analysis method.

For the comparisons here, WACCM was run in the specified dynamics mode, referred to as SD-WACCM (Larmarque et al., 2012). Global assimilated meteorological analyses data from 2002 through 2009 were used to constrain WACCM temperature and horizontal winds in the troposphere and stratosphere. The constraint takes the form of nudging by 1 % at each time step over the altitude range from the surface to 50 km and then a decreasing constraint between 50 and 60 km. Above 60 km, WACCM is free running. The data used for the constraints are from MERRA (Modern Era Retrospective Analysis for Research and Applications). Tidal amplitudes and phases in WACCM were calculated daily using model fields with a time step of 0.5 h. Results from the closest grid point to Ascension Island (15° W and 8.5° S) were interpolated from pressure to geometric height for comparison with the observations.

## 3 Results

### 3.1 Mean winds

Figure 3 presents zonal and meridional hourly winds from March 2009 as a typical example of the MLT wind field over

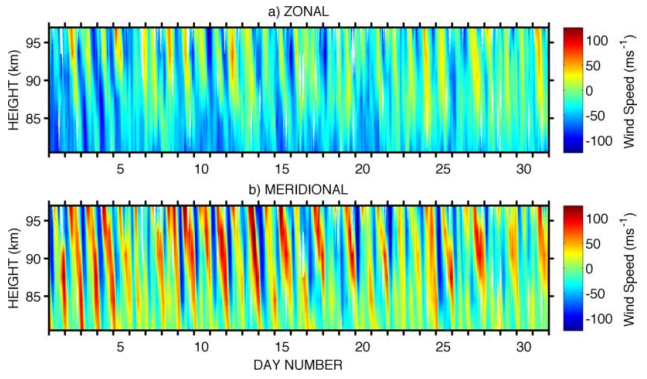


**Fig. 3.** Zonal **(a)** and meridional **(b)** winds as a function of height and time as recorded by the Ascension Island meteor radar in March 2009. The large-amplitude diurnal tide can clearly be seen in both wind components.

Ascension Island. The figure reveals a wind field dominated by the diurnal tide. Instantaneous tidal amplitudes can reach values as large as 130 m s$^{-1}$ (e.g. meridional winds at the upper heights on several occasions throughout the month). The amplitudes are usually significantly smaller at the lowest heights. A clear change of phase with height is evident, with phase fronts descending with time corresponding to an upwardly propagating tide. A high degree of short-term variability is also evident. For instance, meridional tidal amplitudes vary from $\sim$130 m s$^{-1}$ at the upper heights on 14 March to only $\sim$30 m s$^{-1}$ at the same heights on 28 March.

Before we consider the tidal results in detail, we will present the background winds. The composite-year monthly-mean zonal and meridional winds were produced by averaging the mean wind values obtained from the 4-day least-squares fits, and are presented in Fig. 4a and b respectively. In both, the solid line represents the zero-wind line. It can be seen that the zonal winds show the well-known mesospheric semiannual oscillation with the lower four height gates recording predominantly eastward winds at the solstices, and westward winds at the equinoxes. At heights above 93 km however the winds are westward all year. Also of note in the zonal background winds is the strong vertical shear of horizontal wind in the austral winter months. For example, in June and July the wind decreases approximately linearly from around 26 m s$^{-1}$ at heights near 80 km to around $-16$ m s$^{-1}$ at heights near 97 km.

The meridional winds vary less with height than the zonal winds. An annual oscillation is observed, with equatorward winds in the austral summer months at all heights, poleward winds in the austral winter months at all heights and minima at the equinoxes. June and July are again the months of strongest vertical wind shear; however, the variation is much less pronounced than the zonal case, with the mean wind speed decreasing from approximately $-4$ m s$^{-1}$ at heights near 80 km to $-16$ m s$^{-1}$ at heights near 97 km.

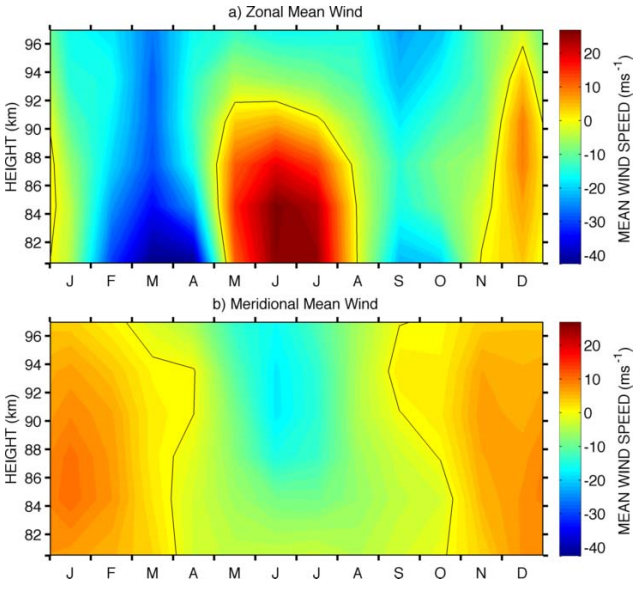


**Fig. 4.** Composite-year monthly-mean winds over Ascension Island for the **(a)** zonal and **(b)** meridional components for all data recorded from January 2002 to June 2011. The black line represents the zero-wind line.

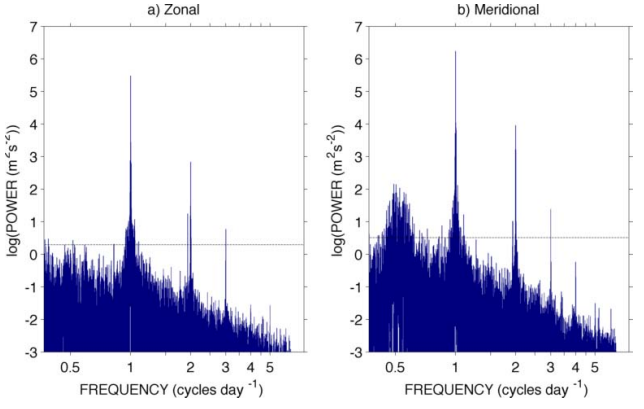


**Fig. 5.** Lomb–Scargle periodograms of the **(a)** zonal and **(b)** meridional wind components at heights near 94 km for the entire set of Ascension Island data (2002–2011). The horizontal dashed lines show the 95 % confidence limit. Note that the strong signal present at 1.93 cycles/day is likely to arise from the lunar semidiurnal tide.

Figure 5a and b present Lomb–Scargle periodograms of zonal and meridional winds, respectively, at a height of 94 km calculated using the entire 2001–2011 dataset.

From the figures it can be seen that there are spectral peaks at frequencies of 1, 2, 3 and 4 cycles per day corresponding to the diurnal, semidiurnal, terdiurnal and quarter-diurnal tides. The figure reveals that the diurnal tide is significantly larger than the other tides. This explains the apparent dominance of the wind field of Fig. 3 by this tide. In this study we will investigate only the diurnal and semidiurnal tides. The

terdiurnal tide also reaches significant amplitudes but will be investigated in a follow-up study.

Also clearly evident in the periodograms of Fig. 5 is a significant oscillation at a frequency of 1.93 cycles per day (corresponding to a period of 12.4 h). This spectral component is most likely to be the lunar semidiurnal tide. The lunar semidiurnal tide as observed by the Ascension Island radar has been described by Sandford et al. (2007) and also observed at low latitudes by Paulino et al. (2012). Alternatively, this spectral signature might result from a non-linear interaction between the semidiurnal tide and the 16-day planetary wave where a "difference frequency wave" would occur at a period of 1.938 cycles per day. However, the persistence of this feature in the long-term spectra and its narrow spectral nature strongly supports the interpretation that it is the lunar semidiurnal tide. Also evident in the figure is a broad maximum in power at frequencies around 0.5 cycles per day. This is taken to result from the 2-day planetary wave which produces maximum amplitudes in meridional winds at low latitudes. We will now turn our attention to the diurnal and semidiurnal tides.

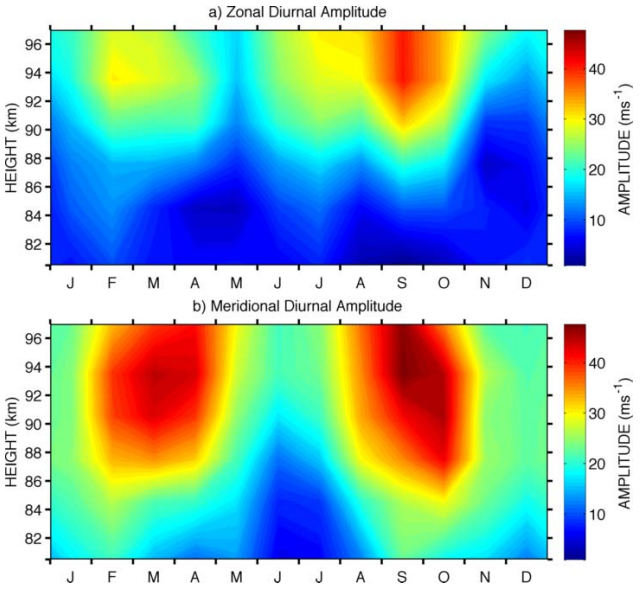


**Fig. 6.** Composite-year monthly-mean diurnal tidal amplitudes as a function of month and height over Ascension Island for all data recorded from January 2002 to June 2011.

### 3.2 Diurnal tide

#### 3.2.1 Amplitudes of the diurnal tide

To investigate the seasonal variability of the diurnal and semidiurnal tides, monthly-mean vector averages were calculated from the 4-day least-squares fits as explained in Sect. 2. The monthly vector-mean amplitudes of the diurnal tide in the zonal and meridional wind components are presented as height–time contours in Fig. 6a and b, respectively. These averages use all available data from January 2002 to June 2011. The diurnal amplitudes in the zonal and meridional components reveal a seasonal cycle. Both components show a semiannual cycle with amplitude maxima at the equinoxes and minima at the solstices. The amplitudes are slightly larger around the austral vernal equinox (September) than the austral autumnal equinox (March). Both zonal and meridional components also show a general increase of amplitude with increasing height. For example, in September amplitudes increase from values of only a few m s$^{-1}$ to $\sim$ 40 m s$^{-1}$ in the zonal component. However, note that amplitudes do not always increase with height. For example, in the zonal component the amplitudes decrease between the top two height gates in April. In the meridional component during the months of largest diurnal tide (February, March, September and October), the amplitudes often maximised at heights around 90 km.

The meridional diurnal amplitudes are generally slightly larger than the zonal. For example, maximum amplitudes reach 48 m s$^{-1}$ in September's meridional winds compared to 41 m s$^{-1}$ in the zonal.

Note that the monthly-mean vector amplitudes shown in the figure smooth out considerable short-term variability. Instantaneous tidal amplitude values can be significantly greater or smaller than these averages (e.g. see Fig. 3).

The data presented in Fig. 6 are presented in Fig. 7 in the form of line plots to enable easier comparison with the model results and to allow the variability of the monthly values of each height gate to be represented. The standard errors on the means of the composite-monthly mean amplitudes and phases were calculated by dividing the standard deviation of all the 4-day least-squares fit values within a month by the square root of the number of values included. These errors thus include both the systematic error and also the natural inter-monthly variation in tidal parameters. The standard errors on the means are generally small. For example they were 1.1 m s$^{-1}$ (amplitude) and 0.3 h (phase) in December 2002, and when averaged over all included months and years the standard errors on the monthly means were found to be 1.3 m s$^{-1}$ and 0.4 h. The "error bars" presented on the plot are the standard deviations of monthly averages and so give a measure of the interannual variability.

The meridional and zonal amplitudes from the radar observations are plotted in Fig. 7a and b respectively. Also presented are the amplitudes predicted by eCMAM and WACCM. These figures confirm the impression given by the height–time contours of Fig. 6 and show that the meridional amplitudes are systematically and significantly larger than the zonal amplitudes in most months. Only in winter (June and July) are the zonal and meridional amplitudes approximately similar. Again, largest amplitudes occur around the equinoxes and smallest amplitudes around the solstices.

Considering the monthly-mean amplitudes predicted by eCMAM, it can be seen that the model predicts significantly

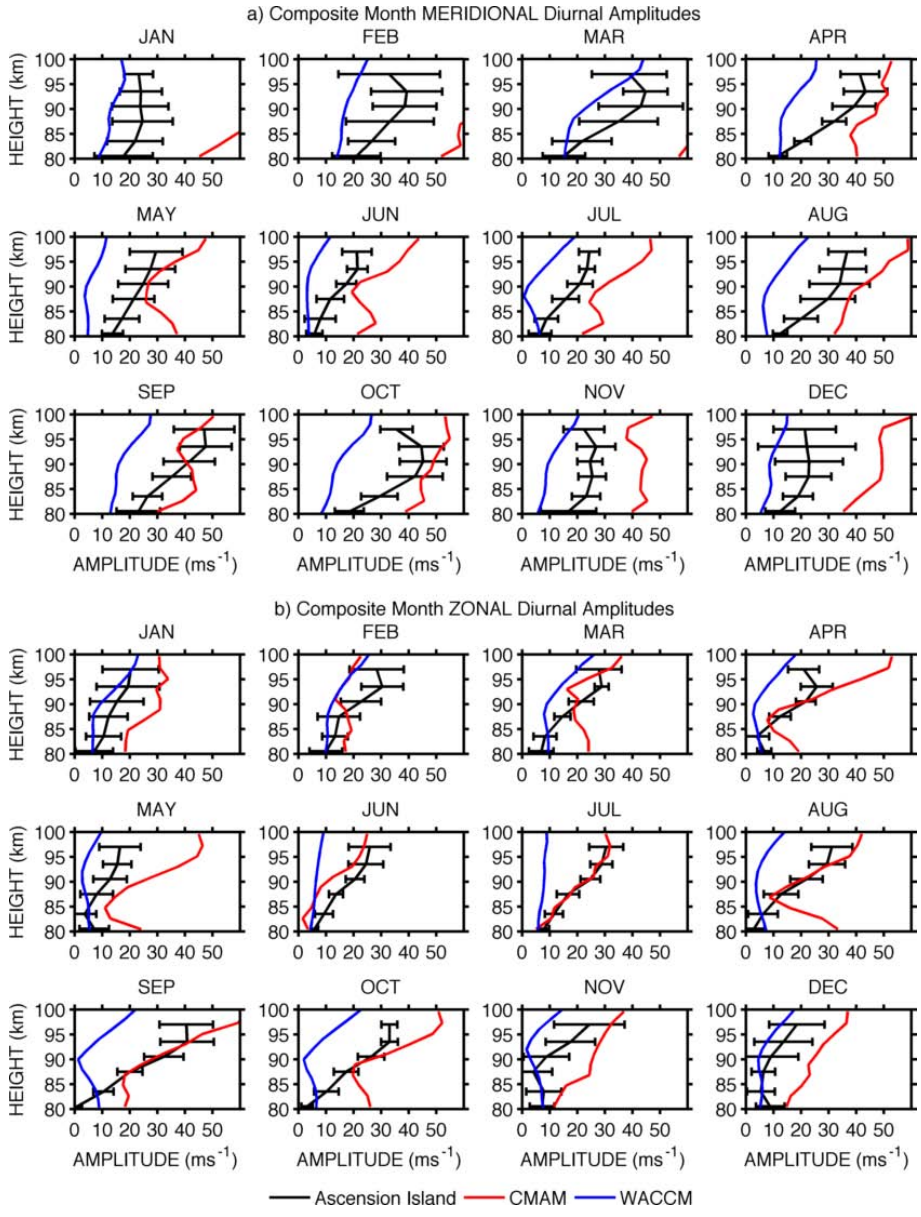


**Fig. 7.** Amplitudes of the **(a)** meridional and **(b)** zonal diurnal tide as a function of month and height. The error bars on the radar observations (black lines) indicate the standard deviation of the individual monthly means over the interval 2002–2011. Also plotted are the predictions of eCMAM (red lines) and WACCM (blue lines).

larger meridional amplitudes than are observed for most months and particularly from November to March. In January to March eCMAM amplitudes reach up to 75 m s$^{-1}$, compared to observed amplitudes of less than 45 m s$^{-1}$ (note that the $x$ axis in the figure has been limited to allow comparison between months and to present the other datasets better). Agreement tends to be better for the zonal component. However, the model again predicts much greater amplitudes than are observed above heights of $\sim$90 km in April, May and October.

Considering the monthly-mean amplitudes predicted by WACCM, it can be seen that the model generally predicts smaller amplitudes than are observed in both zonal and meridional components for most months and heights. This is particularly noticeable in the austral winter/spring months (May–October) when the diurnal amplitudes predicted by WACCM are significantly smaller than observed (sometimes by tens of m s$^{-1}$) and often do not grow with height as rapidly as the observed amplitudes do. The WACCM predictions do, however, reproduce the observed trend of larger diurnal amplitudes in the meridional component than in the

zonal, except for May and June when amplitudes are similar in both components for both the model and the observations.

#### 3.2.2 Phases of the diurnal tide

The linear least-squares fit also returns the phases (the hours of peak amplitude) of the fitted tides. The monthly-mean phases of the diurnal tide are presented as line plots in Fig. 8. As with the corresponding amplitude figure (Fig. 7), the observed phases and model predictions are all shown on the same set of axes for each month. Again, the "error bars" on the plot are the standard deviations of monthly averages and so give a measure of the interannual variability.

The phases as observed over Ascension Island generally show a smooth decrease with increasing height, corresponding to upwardly propagating tides. There are, however, some exceptions. Those exceptions that do occur are between the lowest two height gates in the austral winter months (July and August) where the amplitudes are small and phases thus harder to define. Excluding the lowest height gates in these months of small tidal amplitude, the zonal phases were found to lead the meridional phases by an average of $\sim 6.5$ h, indicating a quadrature relationship.

The phases of the diurnal tide as predicted by eCMAM are similar to the radar observations for both meridional and zonal components for most months. The phases predicted by WACCM are also similar to the radar observations for both meridional and zonal components for most months.

Straight-line least-squares fits to the observed phases as a function of height were used to calculate the vertical wavelengths of the tides as an average over the 80–100 km height interval. These are presented in Table 1. Note that the vertical wavelengths are calculated across all six height gates as an average, and thus local changes in vertical wavelength arising from different tidal modes dominating at different heights are not distinguished. The average vertical wavelengths do however provide a more useful test of the models' ability to reproduce the different modes over one location than the absolute differences in phase.

The zonal vertical wavelengths have values between 20 and 30 km from September through to April (excepting January). However, the vertical wavelengths increase significantly in the winter months from May to August, where the values increase to be between 64 and 111 km. Note that these larger vertical wavelengths in winter result mostly from a reduction in phase hour in the lowest two height gates. Were the phase to be calculated from the May–August data only above heights of 85 km, the vertical wavelengths would be shorter, though still longer than the rest of the year. For example, in May the vertical wavelength calculated above 85 km has a value of $38 \pm 1$ km. The meridional vertical wavelengths are very consistent throughout the year with values ranging only from 24 to 30 km. There is no sign of the increase to larger values evident in the zonal results during winter.

Also presented in Table 1 are the vertical wavelengths derived from the phases predicted by the models. The eCMAM zonal vertical wavelengths are shorter than the observations for every month except November and December. They do however agree within the uncertainty limits for the months of April, October and November. Differences of more than 40 km are evident in May to August (austral winter), months during which the measured vertical wavelengths can greatly exceed those predicted by eCMAM. However, we note that the large zonal vertical wavelengths measured by the radar data in May to August result from the tidal phase having smaller values at the lower height gates yielding a more vertical straight-line fit. If we were to consider data from heights above 85 km only, then the vertical wavelengths would in fact be significantly shorter, ranging from 28 to 47 km. It is interesting to note that other ground-based studies have also observed tidal phase which increases with height at heights near 80 km (e.g. Tsuda et al., 1999; Buriti et al., 2008; Vincent et al., 1998). Considering the meridional wavelengths presented in Table 1, it can be seen that both observations and eCMAM indicate vertical wavelengths to be between 17 and 30 km for all months. The meridional wavelengths predicted by the model are again shorter than those observed, averaging 20 km cf. 26 km respectively.

The WACCM vertical wavelengths are generally in good agreement with the observations. They agree to within the bars representing the interannual variability for all months except January, May, June, August and September in the zonal component. In the meridional component, they agree to within the uncertainty limits for all months except January, June, July and August. Excluding the months with vertical wavelengths of magnitude $\geq 100$ km, the zonal vertical wavelengths predicted by WACCM are slightly shorter on average than those observed, 27 km cf. 29 km, respectively. This is also true for the meridional component, with the WACCM-predicted vertical wavelengths being slightly shorter on average than those observed, 24 cf. 26 km, respectively.

The "error bars" in Fig. 8 are again the standard deviations of monthly means and thus represent the interannual variability. It can be seen that in many months there is actually only a small variation in phase from year to year, indicated by the small error bars. The tidal phases thus appear to repeat from year to year with little variation. The largest standard deviations in the monthly phases tend to be in the zonal component in the lower height gates, possibly due to the corresponding amplitudes being somewhat lower and the phases thus harder to define.

### 3.3 Semidiurnal tide

#### 3.3.1 Amplitudes of the semidiurnal tide

A similar analysis to the above was applied for the semidiurnal tide. The monthly-mean vector-averaged amplitudes

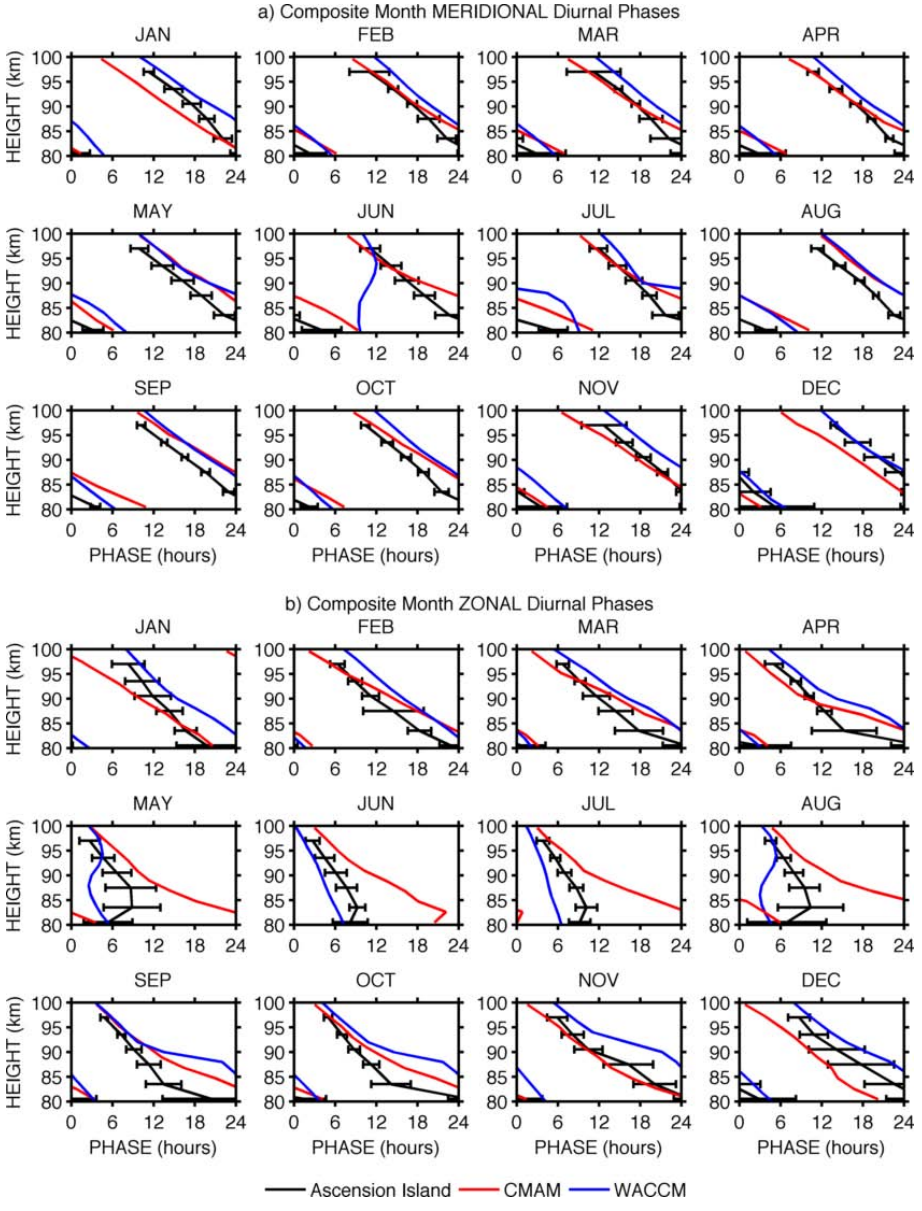


**Fig. 8.** Phases of the **(a)** meridional and **(b)** zonal diurnal tide as a function of month and height. The error bars on the radar observations (black lines) indicate the standard deviation of the individual monthly means over the interval 2002–2011. Also plotted are the predictions of eCMAM (red lines) and WACCM (blue lines).

of the semidiurnal tide in the zonal and meridional wind components are presented in Fig. 9a and b, respectively. The semidiurnal amplitudes are significantly smaller than the diurnal amplitudes, typically reaching values of only 25 % of the diurnal amplitudes (when averaged across all heights and months). In contrast to the diurnal tide, there is a significant difference between the amplitudes of the zonal and meridional components. The meridional amplitudes are generally larger and reach peak values of around 25 m s$^{-1}$, compared to zonal amplitudes of up to around 14 m s$^{-1}$. With the exception of January, the meridional amplitudes are generally about a factor of 3 larger than the zonal amplitudes.

As with the diurnal tide, a strong seasonal variability is apparent. Up to heights of about 90 km, tidal amplitudes exhibit two relatively short-lived maxima: one in April (autumn) and one in October (spring). At heights above 90 km the seasonal variability becomes more complicated with a weaker maximum in amplitude becoming evident in the winter months (June–August). Note also that the zonal amplitudes reach large values around the summer solstice (January) at the upper heights.

A semiannual variability is also evident in the meridional component of the semidiurnal tide amplitudes. Maximum amplitudes occur in March/April and October. A distinct

**Table 1.** Table of the mean diurnal tide vertical wavelengths (km) as observed by the Ascension Island radar (AI) for each month, and the values predicted by eCMAM and WACCM.

| | Zonal $\lambda_z$ (km) | | | Meridional $\lambda_z$ (km) | | |
|---|---|---|---|---|---|---|
| | AI | eCMAM | WACCM | AI | eCMAM | WACCM |
| January | $35 \pm 1$ | $21 \pm 1$ | $21 \pm 1$ | $30 \pm 1$ | $22 \pm 1$ | $25 \pm 1$ |
| February | $24 \pm 1$ | $18 \pm 1$ | $25 \pm 1$ | $27 \pm 1$ | $21 \pm 1$ | $25 \pm 1$ |
| March | $23 \pm 3$ | $17 \pm 1$ | $25 \pm 1$ | $27 \pm 1$ | $20 \pm 1$ | $26 \pm 1$ |
| April | $21 \pm 5$ | $16 \pm 2$ | $22 \pm 1$ | $26 \pm 1$ | $20 \pm 1$ | $26 \pm 1$ |
| May | $100 \pm 15$ | $19 \pm 2$ | $19 \pm 1$ | $24 \pm 1$ | $23 \pm 1$ | $25 \pm 1$ |
| June | $64 \pm 4$ | $23 \pm 1$ | $>100$ | $25 \pm 2$ | $17 \pm 1$ | $20 \pm 1$ |
| July | $66 \pm 4$ | $19 \pm 2$ | $69 \pm 1$ | $25 \pm 3$ | $17 \pm 1$ | $<-100$ |
| August | $>100$ | $17 \pm 2$ | $98 \pm 1$ | $26 \pm 2$ | $21 \pm 1$ | $19 \pm 2$ |
| September | $28 \pm 3$ | $19 \pm 2$ | $<-100$ | $24 \pm 1$ | $18 \pm 1$ | $23 \pm 1$ |
| October | $22 \pm 5$ | $18 \pm 2$ | $17 \pm 2$ | $26 \pm 1$ | $20 \pm 1$ | $24 \pm 1$ |
| November | $20 \pm 2$ | $21 \pm 1$ | $18 \pm 2$ | $27 \pm 1$ | $21 \pm 1$ | $26 \pm 1$ |
| December | $21 \pm 1$ | $26 \pm 1$ | $19 \pm 2$ | $26 \pm 1$ | $22 \pm 1$ | $25 \pm 1$ |

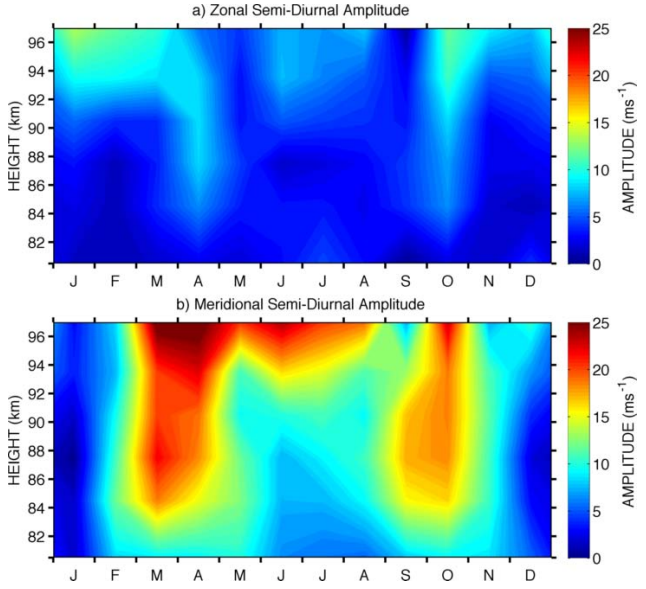


**Fig. 9.** Composite-year monthly-mean semidiurnal tidal amplitudes as a function of month and height over Ascension Island for all data recorded from January 2002 to June 2011.

amplitude minimum occurs around the austral summer solstice (December–January) at all heights. A secondary amplitude minimum occurs in the lower height gates around the austral winter solstice (June–July).

As with the diurnal amplitudes, the data presented in Fig. 9 are presented in Fig. 10 as line plots to enable easier comparison with the model results and to show the interannual variability as indicated by the error bars. For each month the amplitude observations are shown on the same set of axes as the predictions of eCMAM and WACCM.

Considering the monthly-mean amplitudes predicted by eCMAM, it can be seen that there is generally excellent agreement between the predicted amplitudes and the radar observations for the zonal components, except for the month of March when predicted amplitudes are up to $15\,\mathrm{m\,s^{-1}}$ greater than observed amplitudes. In many months, the model predictions lie within the error bars of the observations, at least in some height gates. In the meridional component, agreement is good for most heights in May to September, November and December. eCMAM predicts much smaller amplitudes than are observed in October, and amplitudes to vary much more greatly as a function of height than is observed in February, March and April.

Considering the monthly-mean amplitudes predicted by WACCM, it can be seen that there is generally excellent agreement with the observations in the zonal component, for nearly all months and heights. In the meridional component there is often good agreement, but the model tends to underestimate the amplitudes in March, April, May and September.

### 3.3.2 Phases of the semidiurnal tide

The monthly vector-mean phases of the semidiurnal tide are presented as line plots in Fig. 11. Again, the observations and the model results are all shown on the same set of axes for each month to enable easier comparisons.

It can be seen that there is a clear annual variation in the zonal phases especially in the lower height gates (around 80–90 km) with a maximum of approximately 10:00 LT in the summer months and a minimum of $\sim$ 05:00 LT (or 17:00 LT) in the winter. In the meridional component, there is an annual oscillation in the upper height gates (90–100 km) with a maximum in the winter months and a minimum in the summer, but in the lower height gates the phase stays constant at $\sim$ 10:00 LT throughout the year.

Phases in the zonal component generally decrease with increasing height (i.e. downward phase propagation indicating

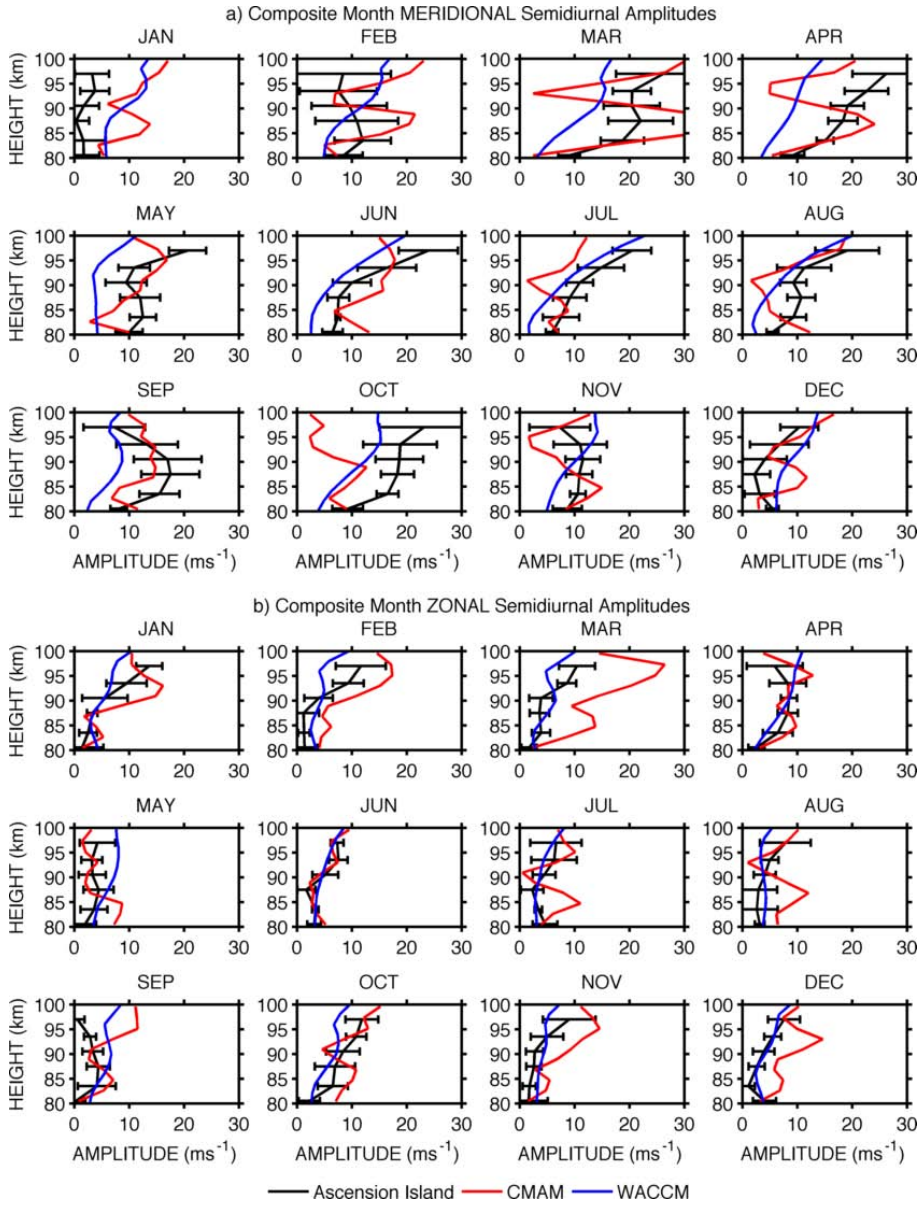


**Fig. 10.** Amplitudes of the **(a)** meridional and **(b)** zonal semidiurnal tide as a function of month and height. The error bars on the radar observations (black lines) indicate the standard deviation of the individual monthly means over the interval 2002–2011. Also plotted are the predictions of eCMAM (red lines) and WACCM (blue lines).

upwards energy flux) in the austral winter months, but are more constant with height in the summer. In contrast, the phases in the meridional component generally decrease with increasing height in the austral summer months, but are more constant with height in the winter.

During the austral winter months, the meridional phases are approximately constant with height, corresponding to very large vertical wavelengths indicating an evanescent semidiurnal tide. The semidiurnal vertical wavelengths calculated from least-squares straight line fits to the phases are presented in Table 2. The semidiurnal vertical wavelengths are found in both wind components to be much longer and with greater month-to-month variability than the diurnal vertical wavelengths.

Considering the monthly-mean semidiurnal phases predicted by eCMAM and the vertical wavelengths that are calculated from them, it can be seen that there is less agreement with the observations than was the case for the diurnal tide. The vertical wavelengths predicted by eCMAM only agree within the uncertainty limits with those observed by the radar for two months for the zonal component, and none for the

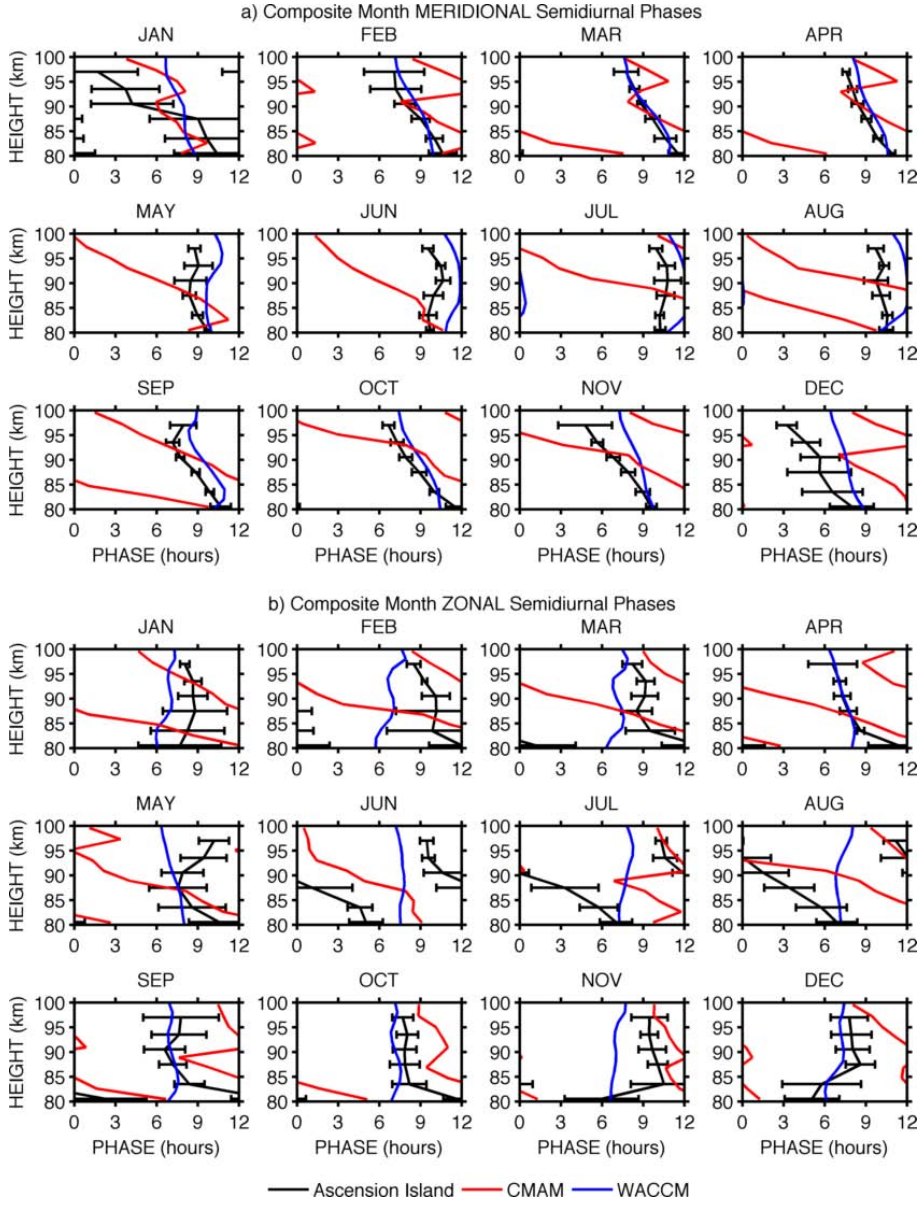


**Fig. 11.** Phases of the **(a)** meridional and **(b)** zonal semidiurnal tide as a function of month and height. The error bars on the radar observations (black lines) indicate the standard deviation of the individual monthly means over the interval 2002–2011. Also plotted are the predictions of eCMAM (red lines) and WACCM (blue lines).

meridional component. Generally, eCMAM tends to predict shorter vertical wavelengths than are observed.

Considering the monthly-mean semidiurnal phases predicted by WACCM and the vertical wavelengths that are calculated from them, it can again be seen that there is less agreement with the observations than there was for the diurnal tide. There is good agreement for some months however. WACCM generally predicts much longer vertical wavelengths than are observed in the zonal component. WACCM also often predicts long vertical wavelengths in the meridional component. However, these WACCM predictions are closer to the observations in April, September, October and December.

### 3.4 Effects of the QBO

To investigate whether or not the phase of the QBO has any effect on diurnal tidal amplitudes, the monthly-mean zonal winds as measured by radiosonde in Singapore were used to define the phase of the QBO (these data are available from http://www.geo.fu-berlin.de/en/met/ag/strat/produkte/qbo). The mesospheric tidal amplitude observations were binned into two sets according to the phase

**Table 2.** Table of the mean semidiurnal tide vertical wavelengths (km) as observed by the Ascension Island radar (AI) for each month, and the values predicted by eCMAM and WACCM.

| | Zonal $\lambda_z$ (km) | | | Meridional $\lambda_z$ (km) | | |
|---|---|---|---|---|---|---|
| | AI | eCMAM | WACCM | AI | eCMAM | WACCM |
| January | $<-100$ | $12\pm1$ | $<-100$ | $21\pm2$ | $66\pm4$ | $>100$ |
| February | $73\pm3$ | $10\pm1$ | $<-100$ | $51\pm1$ | $>100$ | $>100$ |
| March | $54\pm5$ | $11\pm1$ | $<-100$ | $52\pm1$ | $27\pm3$ | $76\pm1$ |
| April | $47\pm3$ | $13\pm1$ | $<-100$ | $60\pm1$ | $30\pm4$ | $61\pm1$ |
| May | $<-100$ | $17\pm2$ | $>100$ | $>100$ | $20\pm2$ | $84\pm1$ |
| June | $22\pm2$ | $22\pm1$ | $>100$ | $<-100$ | $23\pm1$ | $<-100$ |
| July | $20\pm1$ | $<-100$ | $>100$ | $<-100$ | $10\pm1$ | $<-100$ |
| August | $24\pm1$ | $11\pm1$ | $<-100$ | $>100$ | $10\pm1$ | $>100$ |
| September | $39\pm7$ | $49\pm7$ | $<-100$ | $61\pm3$ | $12\pm1$ | $<-100$ |
| October | $68\pm6$ | $38\pm3$ | $>100$ | $42\pm1$ | $11\pm1$ | $97\pm2$ |
| November | $<-100$ | $89\pm3$ | $>100$ | $39\pm1$ | $12\pm1$ | $68\pm1$ |
| December | $-69\pm5$ | $54\pm2$ | $<-100$ | $99\pm10$ | $67\pm2$ | $-92\pm1$ |

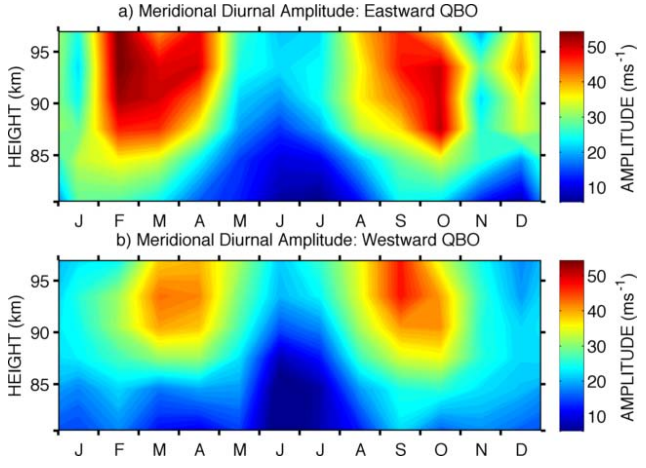


**Fig. 12.** Diurnal tidal amplitudes as a function of month and height for eastward (upper) and westward (lower) QBO phase defined at 10 hPa.

(eastward or westward) of the QBO at 10 hPa and composite months then made. The result of this analysis is two composite years of tidal amplitudes: one for when the QBO was eastward and one for westward. The result for the meridional component of the diurnal tide is shown in Fig. 12.

The figure shows a pronounced effect in which greater amplitudes occur during the eastwards QBO phases than during the westwards QBO phases. For instance, the months February, March and October show an increase in average meridional amplitudes of over $12\,\mathrm{m\,s^{-1}}$ at all heights when the QBO phase is eastward compared to when it is westward. The largest difference in tidal amplitude between eastward and westward phase of the QBO occurs in the top height gate during February when the difference is around $30\,\mathrm{m\,s^{-1}}$. The effect of the QBO phase is smaller for the September equinox than the March equinox. For example, at heights near 87 km in March the diurnal amplitudes increase by approximately 50 % from westward to eastward QBO phase, while in September at the same height the increase is only around 10 %. The effect of the QBO is smaller still for the months of smaller mean amplitude (e.g. at the solstices). Note that while December appears to show an increase in amplitude occurring during eastward QBO phase, there are in fact only two years of observations in December during eastward QBO phases, and so this result may not be significant.

To investigate the effect of the QBO phase on diurnal tidal amplitudes further, the composite-year monthly-mean amplitudes were subtracted from each individual monthly amplitude for the entire dataset. This removes the dominant semi-annual variation in the tidal amplitudes and yields a dataset of perturbations around the annual-mean amplitude behaviour. The results of this analysis for the meridional component at heights near 84 km for the interval 2002–2011 are plotted in Fig. 13. The QBO wind speed at 15 hPa (from the Singapore radiosonde data) is plotted in the same figure. The tidal-amplitude perturbations and mean winds at 15 hPa in this figure have been smoothed using a seven-month running mean to remove short-term fluctuations. The results were only plotted when at least four months of tidal amplitudes were present within each running-mean window, with the missing months set to the mean of the remaining months. Further, recall that monthly-mean tidal amplitudes were only calculated in cases where winds were available for 40 % or more of the hours within a particular month.

Good correlation between the two time series in the figure can be seen by eye, with larger-than-average meridional diurnal amplitudes (positive perturbations) occurring when the QBO winds are eastward, and smaller-than-average meridional diurnal amplitudes when the QBO winds are westward. The correlation coefficient between meridional diurnal

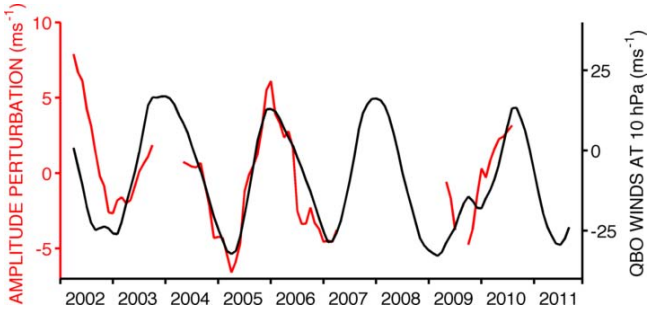


**Fig. 13.** Perturbations in meridional diurnal tide amplitudes (calculated by subtracting the composite-year monthly mean from each individual month) at heights near 84 km for 2002–2011 over Ascension Island (red line). Also plotted are the QBO background winds at 15 hPa (black line). The diurnal tidal amplitude perturbations and background winds are smoothed with a seven-month running mean. Note the two different axes, with the red axis on the left corresponding to the diurnal amplitude perturbations and the black axis on the right corresponding to the QBO line.

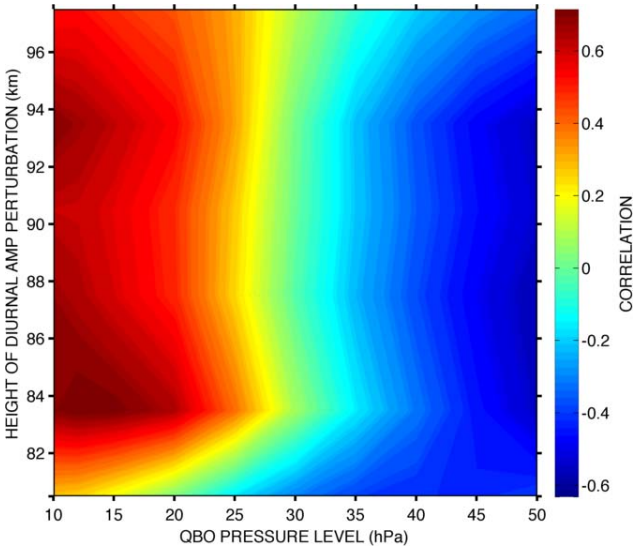


**Fig. 14.** Correlation between meridional diurnal amplitude perturbations and stratospheric QBO winds as a function of height and pressure level.

tidal-amplitude perturbation and the QBO winds for this height gate is 0.72. Note however that strong correlation does not imply causality.

This analysis was repeated such that correlations between amplitude perturbations and QBO winds were obtained for all six radar height gates and for all available pressure levels of QBO winds (between 10 and 50 hPa in the Singapore radiosonde dataset). These correlations are plotted as a function of height and QBO pressure level in Fig. 14.

It can be seen that the meridional diurnal amplitude perturbations at all heights are strongly and positively correlated with QBO winds at pressure levels between 10 and 15 hPa, that there is no correlation with QBO winds defined at around 30 hPa and that there is strong anti-correlation with QBO winds defined at 50 hPa.

To identify the pressure level in the QBO which correlates most strongly with the variability of the mesospheric tides, we calculated the average of the correlations across all radar height gates for each QBO pressure level. This yielded a maximum mean correlation coefficient of 0.58 between meridional diurnal tidal amplitude perturbations and the QBO winds at 10 hPa. This is above the 99 % confidence level and indicates a strong tendency for larger meridional diurnal tidal amplitudes to occur during the eastward phase of the stratospheric QBO at 10 hPa.

This correlation analysis between tidal amplitudes and QBO winds was repeated for the diurnal zonal amplitudes and semidiurnal meridional and zonal amplitudes. These analyses gave mean correlations of 0.21 (at 10 hPa), 0.37 (at 10 hPa) and 0.40 (at 20 hPa), respectively. The bracketed number indicates the QBO pressure level at which highest correlation was obtained for that particular tidal component.

These results appear to indicate a clear connection between the amplitude of certain components of the tropical tide in the upper mesosphere and the phase of the stratospheric QBO winds at a height of 10 hPa. This is particularly noticeable for the meridional component of the diurnal tide.

We performed a similar analysis using the predictions of SD-WACCM. As an example, Fig. 15 presents the meridional diurnal tidal amplitude perturbations at a height of 96 km from WACCM, along with the mean winds at a pressure level of 15 hPa. The correlation between the two can clearly be seen by eye in the figure and has a value of 0.69.

The analysis was repeated for other heights and QBO pressure levels. The resulting correlations are plotted as a function of height and QBO pressure level in Fig. 16 in a similar manner to the observational data presented in Fig. 14.

The figure is remarkably similar to the Ascension Island radar result of Fig. 14, with positive correlation between the meridional diurnal tidal amplitude perturbations and the QBO winds as defined at pressure levels around 10–20 hPa and negative correlations with the QBO winds as defined at pressure levels around 40–50 hPa. When averaged across the 80–100 km height range shown in the figure, the greatest correlation in SD-WACCM is 0.60 with the QBO winds at 18 hPa. This is in excellent agreement with the value of 0.58 at QBO pressure level of 10 hPA observations presented in Fig. 14.

Finally, we note that the QBO is not the only possible cause of the interannual variability observed in the tidal amplitudes. For example, the El Niño Southern Oscillation (ENSO) is a cycle of warmer and cooler Pacific Ocean surface temperatures, which affects atmospheric convection and latent heat release and so may affect the amplitude of atmospheric tides. Over the 2002–2011 interval of this study, the ENSO had a similar period to the QBO. The data of the

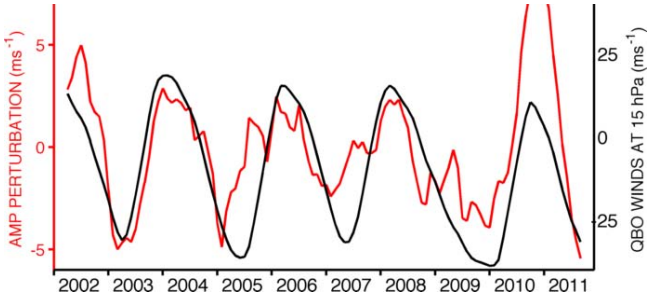


**Fig. 15.** Perturbations in WACCM meridional diurnal tidal amplitudes (calculated by subtracting the composite-year monthly mean from each individual month) at heights near 96 km (red line) for 2002–2011. Also plotted are the QBO background winds at 15 hPa (black line). The diurnal tidal amplitude perturbations and background winds are smoothed with a seven-month running mean. Note the two different axes, with the red axis on the left corresponding to the WACCM diurnal tidal amplitude perturbations and the black axis on the right corresponding to the QBO line.

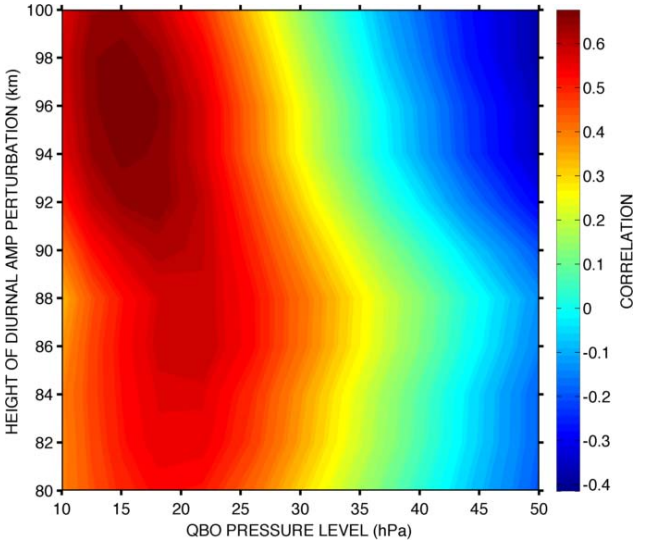


**Fig. 16.** Correlation between WACCM meridional diurnal tidal amplitude perturbations and stratospheric QBO winds as a function of height and pressure level.

standard Niño 3.4 index are presented in Fig. 17. Also plotted in the figure are the meridional diurnal tidal amplitude perturbations (as per Fig. 13). The figure suggests an out-of-phase relationship between the two time series. The correlation coefficient between the two series is found to be $-0.45$. Although smaller in magnitude than the correlation with the QBO, this result nevertheless may indicate a connection between ENSO and tidal amplitudes in the equatorial mesosphere.

### 3.5 Model wavenumber contributions

The model predictions shown here are actually a superposition of a number of different migrating and nonmigrating tidal components. As an example to demonstrate the relative magnitudes and phases of these components, we present in Fig. 18 phasor plots of the contribution from each wavenumber to the total zonal diurnal tide in eCMAM for each month, ranging from wavenumber $s = -5$ to $+5$ at a height of 90 km. Note that the length of each line gives the amplitude of the component, and the phase is given by the angle measured anticlockwise from the positive $x$ axis. Only wavenumbers with amplitudes greater than a threshold of 3 m s$^{-1}$ are shown for each month. Note that we do not show equivalent results for the diurnal meridional and semidiurnal tides for reasons of space.

It is apparent that the W1 migrating tide (blue line) often makes the largest contribution to the eCMAM zonal diurnal tide over Ascension Island. However, for some months (January, February, June, July and September) the amplitude of the E3 component is similar to or even larger than the amplitude of the migrating component. It can also be seen that the phase of the migrating tide does not vary throughout the year as much as the phase of the E3 component.

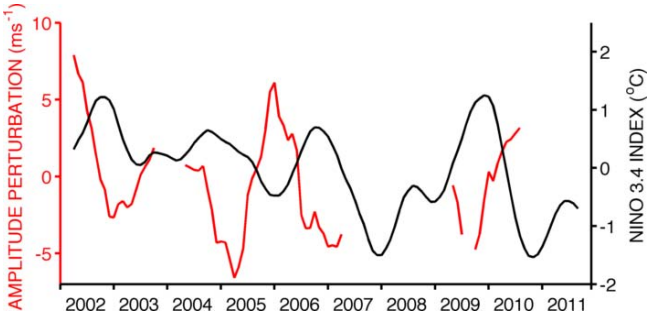


**Fig. 17.** Perturbations in meridional diurnal tide amplitudes (calculated by subtracting the composite-year monthly mean from each individual month) at heights near 84 km (red line) for 2002–2011 over Ascension Island. Also plotted are the data from the Niño 3.4 index (black line), representing sea surface temperature perturbations in the Niño 3.4 Pacific Ocean region. The diurnal tidal amplitude perturbations and Niño 3.4 index are smoothed with a seven-month running mean. Note the two different axes, with the red axis on the left corresponding to the diurnal amplitude perturbations and the black axis on the right corresponding to the Niño 3.4 line.

The results from an equivalent analysis of WACCM output are presented in Fig. 19, but with a lower amplitude threshold of 1.5 m s$^{-1}$ because of the generally lower amplitudes in WACCM.

Again the migrating W1 component (blue line) is the dominant component for most months, with the E3 component also having large magnitude for many months. The E2 component is also large for many months (purple line). It can be seen that for some months (e.g. August–October) even though the migrating component is relatively large, the vector sum with the other components (which are often out of

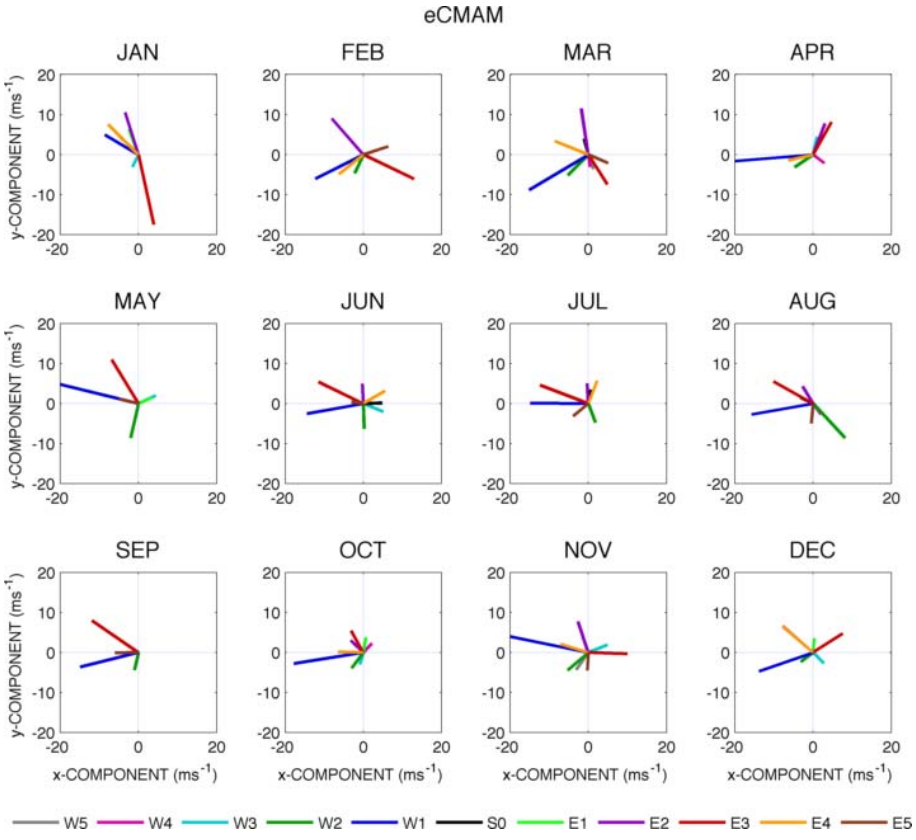


**Fig. 18.** Phasor plots of the individual wavenumbers contributing to the eCMAM-predicted zonal diurnal tide at a height of 90 km. The length of each component represents the magnitude of its contribution, and the angle as measured anticlockwise from the positive $x$ axis gives the phase. Only those components with magnitude greater than $3\,\mathrm{m\,s^{-1}}$ are shown.

phase with the migrating) results in near-zero total amplitude.

Our observations thus indicate that the tidal field over Ascension Island is dominated by a diurnal tide of large amplitude which displays a semiannual seasonal cycle. Tidal amplitudes appear to be modulated by the QBO and also possibly by the ENSO. The model results indicate that the dominant tidal components over Ascension Island are the migrating W1 and the nonmigrating E3 (eCMAM) or the W1, E3 and E2 (WACCM).

## 4 Discussion

The long-term spectra presented in Fig. 5 reveal the dominance of the diurnal and semidiurnal tides in the MLT region over Ascension Island. Planetary and gravity waves over the region can have significant amplitudes, but do not contribute to the long-term spectra as strongly as they are generally either smaller or more intermittent in amplitude than the tides as well as being randomly phased (e.g. Pancheva et al., 2004; Davis et al., 2012).

The results presented in Fig. 6 reveal a very clear semiannual oscillation in the diurnal tidal amplitudes. This seasonal cycle has been reported in other studies (e.g. Deepa et al., 2006; Burrage et al., 1995; McLandress et al., 1996). This semiannual seasonal cycle in the diurnal tidal amplitudes has been attributed by Hagan et al. (1999a) to a seasonal variation of gravity-wave drag on the tide, and these authors were able to model this variation in diurnal tidal amplitudes in the Global Scale Wave Model (GSWM-98). Analysis of CMAM simulations by McLandress (2002a, b) showed that the seasonal variations in the heating that forced the tide and in the structure of the background wind in the stratosphere together accounted for the seasonal cycle in the migrating diurnal tide. However, Xu et al. (2009b) found using TIMED observations that the damping was positively correlated with the tidal winds: the damping was strongest during the equinox periods and so could not explain the observed amplitude variations.

When comparing the Ascension Island results with those from other equatorial sites, the all-sky meteor radar observations from Cariri (7.4° S, 36.5° W) reported by Buriti et al. (2008) are of particular interest due to Cariri's relative proximity to Ascension Island and the similar instrument used. A semiannual cycle in tidal amplitude was observed in the zonal diurnal tides over Cariri between heights of 91 and 98 km, with maxima at the equinoxes. In the meridional

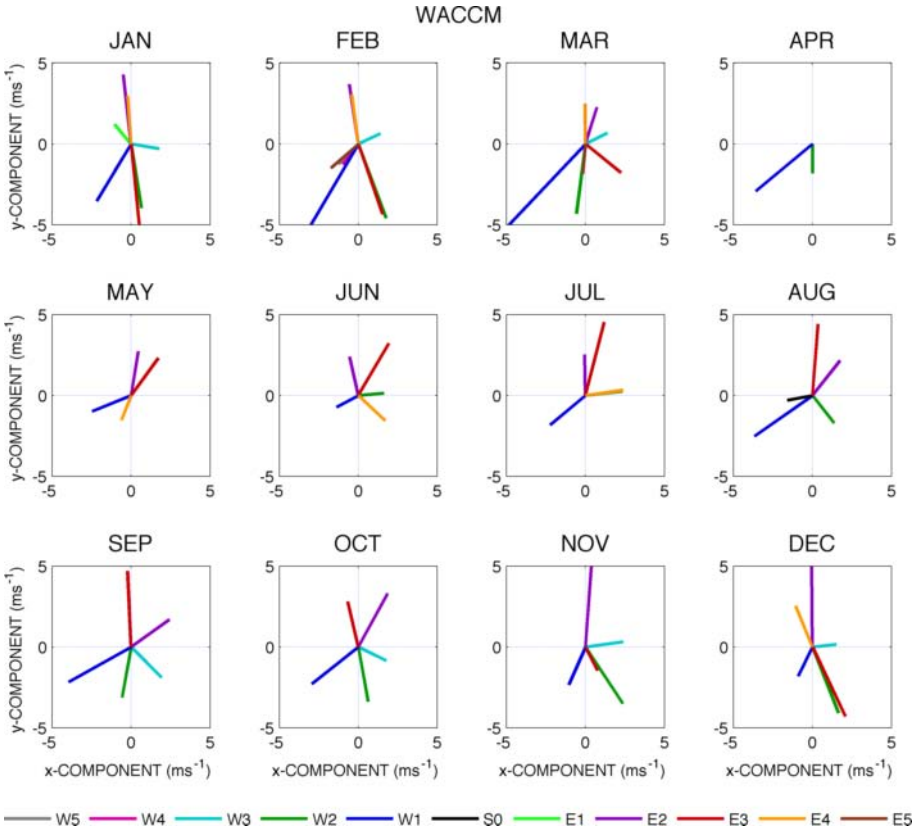


**Fig. 19.** Phasor plots of the individual wavenumbers contributing to the eCMAM-predicted zonal diurnal tide at a height of 90 km. The length of each component represents the magnitude of its contribution, and the angle as measured anticlockwise from the positive $x$ axis gives the phase. Only those components with magnitude greater than $1.5\,\mathrm{m\,s^{-1}}$ are shown.

component, the diurnal amplitudes over Cariri were also observed to have a semiannual cycle with maximum amplitudes at the equinoxes. This behaviour agrees well with that observed over Ascension Island, and the amplitudes are found to be generally similar. There are, however, some differences. For example, the semiannual cycle in amplitudes is observed in the highest height gate of $\sim 97$ km in the Ascension Island meridional diurnal amplitudes but not at the same heights over Cariri. Also, the ratio of meridional amplitudes to zonal amplitudes averaged over all heights and months is observed to be 2 at Cariri, but just 1.6 over Ascension Island.

The diurnal phases between the two sites also have many aspects in common. The average meridional vertical wavelength over Ascension Island is $26 \pm 2$ km, agreeing well with the $23.8 \pm 2.6$ km reported over Cariri. The semidiurnal amplitudes over Cariri generally agree well with those observed over Ascension Island and reported here. The average amplitude over all heights and months at Cariri is $5.8\,\mathrm{m\,s^{-1}}$ in the zonal component and $15.0\,\mathrm{m\,s^{-1}}$ in the meridional component. This compares to Ascension Island's $4.8\,\mathrm{m\,s^{-1}}$ and $11.9\,\mathrm{m\,s^{-1}}$ respectively. Features such as the general increase of amplitude with height and the sharp increase in amplitude between February and March are also observed over both sites. The semidiurnal tidal phases are also generally in good agreement between the two sites.

It should be noted that Buriti et al. (2008) reported results from just one year of observations over Cariri in contrast to the multi-year Ascension Island climatological means reported here. The two sites are separated in latitude by just half a degree, so it would be expected that the *migrating* diurnal tide over Cariri would have similar amplitudes and phases to those over Ascension Island. However, the longitudinal difference of 22.5° between the two sites means that any significant nonmigrating components present may explain the relatively small differences observed between the two sites.

In fact, nonmigrating tides have been proposed to cause large differences in ground-based tidal measurements between two locations at the same latitude. For example, Hagan et al. (1997) found that non-migrating components modelled in the GSWM could reduce the amplitude of the migrating diurnal tide in the low-latitude Pacific, accounting for the large observational differences between the radar situated on Kauai and the migrating tidal amplitudes from satellite observations. Chang et al. (2010) examined diurnal tidal amplitudes from three sites at approximately equivalent

latitudes near 22° S. These were Learmonth (23° S, 114° E), Rarotonga (22° S, 160° W), and Cachoeira Paulista (23° S, 45° W). They compared these amplitudes with the predictions of four models (WACCM, eCMAM, TIME-GCM and the GSWM-02). They found significant differences in amplitude between the three sites due to differing superpositions of migrating and non-migrating tides. They also found that while the models failed to reproduce the observed longitudinal differences accurately, a common general pattern of zonal variation was observed in three of the models. The importance of the longitudinal structure of the tides was discussed in detail by Ward et al. (2010). However, the superposition of tidal components deduced from TIDI observations presented by these authors reveals that Ascension Island happens to be in a region of comparatively constant tidal amplitude as a function of longitude. This would again help explain the similarities between the Ascension Island and Cariri observations. Our results in comparison with those from Cariri reported by Buriti et al. (2008) thus support the conclusions of Ward et al. (2010).

Other comparisons of particular interest are with the results of Deepa et al. (2006) from the radar at Trivandrum (8.5° N, 77° E), approximately at Ascension Island's conjugate latitude. Again the results were obtained from an all-sky meteor radar, and so instrumental differences should be negligible. Deepa et al. (2006) observed the diurnal amplitudes to be larger than the semidiurnal and the meridional components for both tides to be larger than the zonal. They also observed a semiannual cycle in diurnal amplitudes with maxima around the equinoxes in the zonal component. These observations agree well with the observations presented here from Ascension Island. However, in the meridional component, at heights above 90 km Deepa et al. (2006) observed an annual cycle in tidal amplitudes with maxima in the winter months and minima in the summer in contrast to the semiannual cycle with equinoctial maxima observed. The mean amplitudes were slightly larger than those observed over Ascension Island, with peak amplitudes of $\sim 60\,\mathrm{m\,s^{-1}}$, cf. $48\,\mathrm{m\,s^{-1}}$ over Ascension Island. Vertical wavelengths in both zonal and meridional components were found to be $\sim 25$ km, similar to the Ascension Island results.

Deepa et al. (2006) also observed slightly larger semidiurnal amplitudes than are observed over Ascension Island. The vertical wavelengths observed were generally similar to the Ascension Island results. They attributed the presence of vertical wavelengths greater than 100 km to the dominance of the (2,2) mode as predicted by Forbes (1982).

We will now consider the results from eCMAM and WACCM. In the case of comparisons of eCMAM with observations, it has been noted in previous studies that the amplitudes of the eastward-propagating tidal components in eCMAM are much larger than the values observed by the TIMED Doppler Interferometer (TIDI), while westward propagating components are of comparable magnitudes (Du et al., 2007; Du, 2008; Chang et al., 2010). It is therefore possible that eCMAM overestimates the parameterizations of latent heat release and deep convection responsible for generating the eastward-propagating tidal components.

It is known that tidal vertical wavelengths are affected by eddy diffusion and momentum deposition in the MLT from gravity-wave breaking (Ortland and Alexander, 2006). The slightly shorter vertical wavelengths in the eCMAM compared to our observations may thus be a result of in-phase gravity-wave momentum forcing, commonly associated with the Hines parameterization employed in the model (McLandress, 2002a).

Further, differences could also be caused by differences between the actual tidal sources during the time period of the radar observations compared to the tidal sources in the model. Differences could also be caused by differences in the background atmosphere between that used in the model and the real atmosphere, which would result in differences in the propagation conditions for the component and/or Hough mode. Finally, since only one year of model data is used in these comparisons, year-to-year variations in the model may also play a role. Given these uncertainties, it is striking that the agreement is as good as reported here.

The most consistent of the differences between the WACCM simulations and the observations are the lower amplitudes in WACCM. Since SD-WACCM nudges to observational data in the troposphere and stratosphere, the differences are likely not due to tidal heating or other tidal sources. However, there are several processes that could contribute to these differences. Firstly, the tidal amplitudes may be suppressed in the MERRA analyses used for the nudging because the meteorological data used in the assimilation are ingested at infrequent intervals, thus damping high-frequency variability such as tides. It is also possible that the conditions for tidal propagation in WACCM (background winds and temperatures in the mesosphere) are incorrect, or that tides in WACCM are excessively damped by parameterized gravity-wave processes. Finally, insufficient vertical resolution in the mesosphere could also affect the simulation of the tides. In general, tidal amplitudes in WACCM that are systematically too low are a known problem that is currently under investigation (Smith, 2012).

Our results (Figs. 18 and 19) show that the dominant wavenumbers contributing to the total zonal diurnal tidal field in both eCMAM and WACCM are the migrating W1 and the nonmigrating E3. The figures also highlight one of the difficulties models face in attempting to predict tidal amplitudes and phases accurately. With many wavenumbers contributing to the total tidal field, identifying whether differences between the observed tidal field and the model predictions are due to, for example, the overestimation of the amplitude of one component, or the underestimation of another, or the incorrect phase of a third, etc. becomes very difficult. A useful step towards solving some of these problems might involve studies made with chains of radars at approximately equal latitudes, or alternatively studies focusing on satellite

data, which would be able to distinguish wavenumbers but at the price of poorer time resolution.

Our observations (e.g. Fig. 14) indicate that the QBO appears to influence the amplitudes of the diurnal tidal in the MLT, with larger amplitudes occurring when the QBO wind at 10 hPa is eastward. This connection has been reported in a limited number of other studies, for example Vincent et al. (1998). However, it should be noted that the positive correlation we report here does not necessarily imply that any mechanism linking the QBO and tidal amplitudes exists at heights around 10 hPa.

The correlations between QBO wind at 10 hPa and tidal-amplitude perturbations reported in Sect. 3.4 show that the correlation (averaged across all radar height gates) is higher for the meridional diurnal tidal amplitudes (0.58) than the semidiurnal (0.37). This greater effect of the QBO on the meridional diurnal amplitudes compared to the effect on the meridional semidiurnal amplitudes provides support to similar conclusions drawn from the TIDI/TIMED satellite observations reported by Wu et al. (2011).

Hagan et al. (1999b) performed a number of numerical experiments with the GSWM-98 to investigate two possible causes of this QBO modulation of MLT diurnal tidal amplitudes. These causes were (i) the QBO in zonal-mean zonal winds and (ii) variable forcing arising from the QBO in stratospheric ozone. They suggested that the QBO in zonal-mean zonal winds cause variations in tidal amplitude by approximately 40 %, somewhat larger than what we observe over Ascension Island. They also concluded that the QBO in stratospheric ozone has negligible effect on MLT diurnal tidal amplitudes because the major ozone variations occur below the height of the majority of the ozone heating. Mayr and Mengel (2005) were able to produce a QBO with realistic periods in a numerical spectral model and found that it can modulate tidal amplitudes by up to 30 %. They found that at heights above 80 km this modulation was driven by gravity-wave momentum deposition.

However, in contrast, Xu et al. (2009a) came to a different conclusion about the role of gravity waves. They found that the tropical zonal wind variations associated with the QBO had little effect on the filtering of gravity waves because the effect was masked by the larger magnitude winds in the upper stratosphere. As of now, there is thus no consensus on the processes that are responsible for the QBO variation in tidal amplitudes.

Our results (Fig. 17) show that the observed mesospheric tidal amplitudes over Ascension Island have negative correlation with the ENSO index. This is particularly interesting when contrasted with the enhanced diurnal amplitudes in the MLT observed during El Niño events, i.e. positive correlations, at various ground-based stations in the Pacific (Tirunelveli, Jakarta, Kauai, and Christmas Island) as observed by Gurubaran et al. (2005) and Lieberman et al. (2007). This is the opposite of the effect we observe over Ascension Island. However, the regional impact of ENSO can be very complicated, and further analysis would require decomposing the observed tides into migrating and non-migrating components. This would allow an examination of how water vapour and latent heat release change both globally and locally during El Niño and La Niña events and how these affect tides in the mesosphere. The relative impact of the QBO and the ENSO on tidal amplitudes in the mesosphere remains an interesting question.

## 5 Conclusions

Ten years (2002–2011) of wind observations from the Ascension Island meteor radar (8° S, 14° W) have been analysed to characterise the diurnal and semidiurnal tides over the tropical mid-Atlantic region. The length of the dataset enables an investigation into the effect of the stratospheric QBO on the tidal amplitudes. Comparisons have been made between the observed tidal parameters and those predicted by the eCMAM and WACCM models.

The MLT wind field over Ascension Island has been shown to be dominated by the diurnal tide, which can have instantaneous amplitudes on occasion reaching in excess of $100\,\mathrm{m\,s^{-1}}$. The semidiurnal tide is also present but smaller in amplitude.

Considering the diurnal tide over the height range observed, monthly-mean diurnal amplitudes generally increase with height. In both zonal and meridional components of the diurnal tide, there is a semiannual seasonal variation apparent, with amplitude maxima at the equinoxes and amplitude minima at the solstices. Amplitudes are greater in the meridional component than the zonal for all months except the low-amplitude austral winter months of June and July. The meridional diurnal tidal vertical wavelengths are generally similar throughout the year, ranging from 24 to 30 km. The zonal vertical wavelengths are generally similar to the meridional, except for during the austral winter months when the zonal vertical wavelengths are much longer.

Semidiurnal tidal amplitudes are observed to be approximately 25 % of the diurnal amplitudes (when averaged across all heights and months). There is a greater difference in amplitude between the meridional and zonal components of the semidiurnal tide than was the case with the diurnal tide. The semidiurnal tidal vertical wavelengths vary much more than is the case for the diurnal tide.

Both eCMAM and WACCM reproduce the trend for greater diurnal amplitudes in the meridional component than the zonal. However, eCMAM tends to overpredict meridional amplitudes, while WACCM underpredicts zonal and meridional amplitudes. Semidiurnal amplitude predictions were generally good for both models. Vertical wavelength predictions were also often good for both models. However, eCMAM predicts shorter zonal vertical wavelengths than observed for the diurnal tide in austral winter, while WACCM

predicts longer zonal semidiurnal vertical wavelengths than observed for most months.

Component analysis of the eCMAM and WACCM zonal diurnal tide shows that the migrating W1 and the nonmigrating E3 components were the dominant contributors to the total tidal field.

Finally, sorting MLT region tidal amplitudes by QBO phase at 10 hPa revealed that larger-than-average meridional diurnal amplitudes occur when the stratospheric QBO winds are eastwards, and smaller-than-average meridional diurnal amplitudes occur when the QBO winds are westwards. Correlations show that the QBO appears to have the most effect on the diurnal tide in the meridional component. Despite the significant magnitude of QBO modulation of tidal amplitudes, there appears to be no consensus as to the underlying physical cause. The similar period of the ENSO during the 2002–2011 interval further complicates the issue. This highlights the need for further studies on the coupling between the ENSO, the stratospheric QBO and the tides of the MLT.

*Acknowledgements.* The National Center for Atmospheric Research is sponsored by the National Science Foundation. We would like to thank one of the anonymous reviewers for their suggestion that we consider ENSO as a possible cause of the interannual variability in tidal amplitudes.

Edited by: F.-J. Lübken

## References

Andrioli, V. F., Clemesha, B. R., Batista, P. P, and Schuch, N. J.: Atmospheric tides and mean winds in the meteor region over Santa Maria (29.71° S; 53.81° W), J. Atmos. Sol. Terr. Phys., 71, 1864–1876, 2009.

Avery, S. K., Vincent, R. A., Phillips, A., Manson, A. H., and Fraser, G. J.: High-latitude tidal behaviour in the mesosphere and lower thermosphere, J. Atmos. Terr. Phys., 51, 595–608, doi:10.1016/0021-9169(89)90057-3, 1989.

Beard, A. G., Mitchell, N. J., Williams, P. J. S., and Kunitake, M.:Non-linear interactions between tides and planetary waves resulting in periodic tidal variability, J. Atmos. Sol. Terr. Phys., 61, 363–376, doi:10.1016/S1364-6826(99)00003-6, 1999.

Beldon, C. L. and Mitchell, N. J.: Gravity wave-tidal interactions in the mesosphere and lower thermosphere over Rothera, Antarctica (68 degrees S, 68 degrees W), J. Geophys. Res.-Atmos., 115, D18101, doi:10.1029/2009JD013617, 2010.

Buriti, R. A., Hocking, W. K., Batista, P. P., Medeiros, A. F., and Clemesha, B. R.: Observations of equatorial mesospheric winds over Cariri (7.4° S) by a meteor radar and comparison with existing models, Ann. Geophys., 26, 485–497, doi:10.5194/angeo-26-485-2008, 2008.

Burrage, M. D., Hagan, M. E., Skinner, W. R., Wu, D. L., and Hays, P. B.: Long-term variability in the solar diurnal tide observed by HRDI and simulated by the GSWM, Geophys. Res. Lett., 22, 2641–2644, doi:10.1029/95GL02635, 1995.

Chang, J. L. and Avery, S. K.: Observations of the diurnal tide in the mesosphere and lower thermosphere over Christmas Island, J. Geophys. Res.-Atmos., 102, 1895–1907, 1997.

Chang, L. C., Ward, W. E., Palo, S. E., Du, J., Wang, D.-Y, Liu, H.-L., Hagan, M. E., Portnyagin, Y., Oberheide, J., Goncharenko, L. P., Nakamura, T., Homann, P., Singer, W., Batista, P., Clemesha, B., Manson, A. H., Riggin, D. M., She, C.-Y., Tsuda, T., and Yuan, T.: Comparison of diurnal tide in models and ground-based observations during the 2005 equinox CAWSES tidal campaign, J. Atmos. Sol. Terr. Phys., 78, 19–30, doi:10.1016/j.jastp.2010.12.010, 2010.

Chang, L. C., Palo, S. E., and Liu, H. L.: Short-term variability in the migrating diurnal tide caused by interactions with the quasi 2 day wave, J. Geophys. Res.-Atmos., 116, D12112, doi:10.1029/2010JD014996, 2011.

Chu, X. Z., Gardner, C. S., and Papen, G.: Lidar observations of polar mesospheric clouds at South Pole: Diurnal variations, Geophys. Res. Lett., 28, 1937–1940, doi:10.1029/2000GL012525, 2001.

Davis, R. N., Chen, Y.-W., Miyahara, S., and Mitchell, N. J.: The climatology, propagation and excitation of ultra-fast Kelvin waves as observed by meteor radar, Aura MLS, TRMM and in the Kyushu-GCM, Atmos. Chem. Phys., 12, 1865–1879, doi:10.5194/acp-12-1865-2012, 2012.

Deepa, V., Ramkumar, G., Antonita, M., Kumar, K. K., and Sasi, M. N.: Vertical propagation characteristics and seasonal variability of tidal wind oscillations in the MLT region over Trivandrum (8.5° N, 77° E): first results from SKiYMET Meteor Radar, Ann. Geophys., 24, 2877–2889, doi:10.5194/angeo-24-2877-2006, 2006.

Du, J.: A mesosphere and lower thermosphere dynamics study using the extended Canadian Middle Atmosphere Model (CMAM), University of New Brunswick (Canada), 2008.

Du, J. and Ward, W. E.: Terdiurnal tide in the extended Canadian Middle Atmospheric Model (CMAM), J. Geophys. Res.-Atmos., 115, D24106, doi:10.1029/2010JD014479, 2010.

Du, J., Ward, W. E., Oberheide, J., Nakamura, T., and Tsuda, T.: Semidiurnal tides from the Extended Canadian Middle Atmosphere Model (CMAM) and comparisons with TIMED Doppler Interferometer (TIDI) and meter radar observations, J. Atmos. Sol. Terr. Phys., 69, 2159–2202, doi:10.1016/j.jastp.2007.07.014, 2007.

Fiedler, J., Baumgarten, G., and von Cossart, G.: Mean diurnal variations of noctilucent clouds during 7 years of lidar observations at ALOMAR, Ann. Geophys., 23, 1175–1181, doi:10.5194/angeo-23-1175-2005, 2005.

Fomichev, V. I., Ward, W. E., Beagley, S. R., McLandress, C., McConnell, J. C., McFarlane, N. A., and Shepherd, T. G.: Extended Canadian Middle Atmosphere Model: Zonal-mean climatology and physical parameterizations, J. Geophys. Res., 107, 4087, doi:10.1029/2001JD000479, 2002.

Forbes, J. M.: Atmospheric tides. 1: Model description and results for the solar diurnal component, J. Geophys. Res., 87, 5222–5240, doi:10.1029/JA087iA07p05222, 1982.

Forbes, J. M. and Moudden, Y.: Quasi-two-day wave-tide interactions as revealed in satellite observations, J. Geophys. Res.-Atmos., 117, D12110, doi:10.1029/2011JD017114, 2012.

Fraser, G. J., Portnyagin, Y. I., Forbes, J. M., Vincent, R. A., Lysenko, I. A., and Makarov, N. A.: Diurnal tide in the Antarctic

and Arctic mesosphere/lower thermosphere regions, J. Atmos. Terr. Phys., 57, 383–393, 1995.

Friedman, J. S., Zhang, X., Chu, X., and Forbes, J. M.: Longitude variations of the solar semidiurnal tides in the mesosphere and lower thermosphere at low latitudes observed from ground and space, J. Geophys. Res.-Atmos., 114, D11114, doi:10.1029/2009JD011763, 2009.

Fritts, D. C. and Isler, J. R.: Mean motions and tidal and two-day structure and variability in the mesosphere and lower thermosphere over Hawaii, J. Atmos. Sci., 51, 2145–2164, 1994.

Fritts, D. C. and Vincent, R. A.: Mesospheric momentum flux studies at Adelaide, Australia: Observations and a gravity wave/tidal interaction model, J. Atmos. Sci., 44, 605–619, 1987.

Gurubaran, S., Rajaram, R., Nakamura, T., and Tsuda, T.: Interannual variability of diurnal tide in the tropical mesopause region: A signature of the El Nino-Southern Oscillation (ENSO), Geophys. Res. Lett., 32, L13805, doi:10.1029/2005GL022928, 2005.

Gurubaran, S., Rajaram, R., Nakamura, T., Tsuda, T., Riggin, D., and Vincent, R. A.: Radar observations of the diurnal tide in the tropical mesosphere-lower thermosphere region: Longitudinal variabilities, Earth Planets Space, 61, 513–524, 2009.

Hagan, M. E. and Forbes, J. M.: Migrating and nonmigrating ssemidiurnal tides in the upper atmosphere excited by tropospheric latent heat release, J. Geophys. Res.-Atmos., 108, 1062, doi:10.1029/2002JA009466, 2003.

Hagan, M. E., McLandress, C., and Forbes, J. M.: Diurnal tidal variability in the upper mesosphere and lower thermosphere, Ann. Geophys., 15, 1176–1186, doi:10.1007/s00585-997-1176-x, 1997.

Hagan, M. E., Burrage, M. D., Forbes, J. M., Hackney, J., Randel, W. J., and Zhang, X.: GSWM-98: Results for migrating solar tides, J. Geophys. Res., 104, 6813–6828, 1999.

Hagan, M. E., Burrage, M. D., Forbes, J. M., Hackney, J., Randel, W. J., and Zhang, X.: QBO effects on the diurnal tide in the upper atmosphere, Earth Planets Space, 51, 571–578, 1999.

Hays, P. B. and Wu, D. L.: Observations of the diurnal tide from space, J. Atmos. Sci., 51, 3077–3093, 1994.

Hines, C. O.: Doppler spread parameterization of gravity wave momentum deposition in the middle atmosphere. Part 1. Basic formulation, J. Atmos. Sol. Terr. Phys., 59, 371–386, doi:10.1016/S1364-6826(99)00058-9, 1997.

Hines, C. O.: Doppler spread parameterization of gravity wave momentum deposition in the middle atmosphere. Part 2. Broad and quasimonochromatic spectra, and implementation, J. Atmos. Sol. Terr. Phys., 59, 387–400, doi:10.1016/S1364-6826(96)00080-6, 1997.

Immel, T. J., Sagawa, E., England, S. L., Henderson, S. B., Hagan, M. E., Mende, S. B., Frey, H. U., Swenson, C. M., and Paxton, L. J.: Control of equatorial ionospheric morphology by atmospheric tides, Geophys. Res. Lett., 33, L15108, doi:10.1029/2006GL026161, 2006.

Kumar, K. K., Deepa, V., Antonita, T. M., and Ramkuma, G.: Meteor radar observations of short-term tidal variabilities in the low-latitude mesosphere-lower thermosphere: Evidence for nonlinear wave-wave interactions, J. Geophys. Res., 113, D16108, doi:10.1029/2007JD009610, 2008.

Lamarque, J.-F., Emmons, L. K., Hess, P. G., Kinnison, D. E., Tilmes, S., Vitt, F., Heald, C. L., Holland, E. A., Lauritzen, P. H., Neu, J., Orlando, J. J., Rasch, P. J., and Tyndall, G. K.: CAM-chem: description and evaluation of interactive atmospheric chemistry in the Community Earth System Model, Geosci. Model Dev., 5, 369–411, doi:10.5194/gmd-5-369-2012, 2012.

Lieberman, R. S. and Hays, P. B.: An estimate of the momentum deposition in the lower thermosphere by the observed diurnal tide, J. Atmos. Sci., 51, 3094–3105, 1994.

Lieberman, R. S., Riggin, D. M., Ortland, D. A., Nesbitt, S. W., and Vincent, R. A.: Variability of mesospheric diurnal tides and tropospheric diurnal heating during 1997-1998, J. Geophys. Res.-Atmos., 112, D20110, doi:10.1029/2007JD008578, 2007.

Lindzen, R. S.: Thermally driven diurnal tide in atmosphere, Q. J. Roy. Meteor. Soc., 93, 18–42, doi:10.1002/qj.49709339503, 1967.

Lindzen, R. S. and Chapman, S.: Atmospheric Tides, Sp. Sci. Revs., 10, 3–188, 1969.

Manson, A. H., Meek, C. E., Avery, S. K., and Tetenbaum, D.: Comparison of mean wind and tidal fields at Saskatoon (52° N, 107° W) and Poker Flat (65° N, 147° W) during 1983/1984, Phys. Scripta, 37, 169–177, 1988.

Manson, A. H., Meek, C. E., Teitelbaum, H., Vial, F., Schminder, R., Kurschner, D., Smith, M. J., Fraser, G. J., and Clark, R. R.: Climatologies of semi-diurnal and diurnal tides in the middle atmosphere (70–110 km) at middle latitudes (40–55-degrees), J. Atmos. Terr. Phys., 51, 579–593, doi:10.1016/0021-9169(89)90056-1, 1989.

Manson, A., Meek, C., Hagan, M., Hall, C., Hocking, W., MacDougall, J., Franke, S., Riggin, D., Fritts, D., Vincent, R., and Burrage, M.: Seasonal variations of the semi-diurnal and diurnal tides in the MLT: multi-year MF radar observations from 2 to 70N, and the GSWM tidal model, J. Atmos. Sol. Terr. Phys., 61, 809–828, 1999.

Manson, A. H., Meek, C. E., Chshyolkova, T., Xu, X., Aso, T., Drummond, J. R., Hall, C. M., Hocking, W. K., Jacobi, Ch., Tsutsumi, M., and Ward, W. E.: Arctic tidal characteristics at Eureka (80° N, 86° W) and Svalbard (78° N, 16° E) for 2006/07: seasonal and longitudinal variations, migrating and non-migrating tides, Ann. Geophys., 27, 1153–1173, doi:10.5194/angeo-27-1153-2009, 2009.

Mayr, H. G. and Mengel, J. G.: Interannual variations of the diurnal tide in the mesosphere generated by the quasi-biennial oscillation, J. Geophys. Res.-Atmos., 110, D10111, doi:10.1029/2004JD005055, 2005.

McLandress, C.: The seasonal variation of the propagating diurnal tide in the mesosphere and lower thermosphere: Part I The role of gravity waves and planetary waves, J. Atmos. Sci., 59, 893–906, 2002.

McLandress, C.: The seasonal variation of the propagating diurnal tide in the mesosphere and lower thermosphere: Part II The role of tidal heating and zonal mean winds, J. Atmos. Sci., 59, 907–922, 2002.

McLandress, C., Shephard, G. G., and Solheim, B. H.: Satellite observations of thermospheric tides: Results from the Wind Imaging Interferometer on UARS, J. Geophys. Res., 101, 4093–4114, 1996.

Mitchell, N. J., Pancheva, D., Middleton, H. R., and Hagan, M. E.: Mean winds and tides in the Arctic mesosphere and lower thermosphere, J. Geophys. Res.-Atmos, 107, 1004, doi:10.1029/2001JA900127, 2002.

Miyahara, S., Yoshida, Y., and Miyoshi, Y.: Dynamic coupling between the lower and upper-atmosphere by tides and gravity waves, J. Atmos. Terr. Phys., 55, 1039–1053, doi:10.1016/0021-9169(93)90096-H, 1993.

Oberheide, J., Hagan, M. E., Roble, R. G., and Offermann, D.: Sources of nonmigrating tides in the tropical middle atmosphere, J. Geophys. Res.-Atmos., 107, 4567, doi:10.1029/2002JD002220, 2002.

Oberheide, J., Wu, Q., Killeen, T. L., Hagan, M. E., and Roble, R. G.: Diurnal nonmigrating tides from TIMED Doppler Interferometer wind data: Monthly climatologies and seasonal variations, J. Geophys. Res.-Space, 111, A10S03, doi:10.1029/2005JA011491, 2006.

Oberheide, J., Wu, Q., Killeen, T. L., Hagan, M. E., and Roble, R. G.: A climatology of nonmigrating semidiurnal tides from TIMED Doppler Interferometer (TIDI) wind data, J. Atmos. Sol. Terr. Phys., 69, 2202–2218, doi:10.1016/j.jastp.2007.05.010, 2007.

Ortland, D. A. and Alexander, M. J.: Gravity wave influence on the global structure of the diurnal tide in the mesosphere and lower thermosphere, J. Geophys. Res., 22, A10S10, doi:10.1029/2005JA011467, 2006.

Pancheva, D., Mitchell, N. J., and Younger, P. T.: Meteor radar observations of atmospheric waves in the equatorial mesosphere/lower thermosphere over Ascension Island, Ann. Geophys., 22, 387–404, doi:10.5194/angeo-22-387-2004, 2004.

Pancheva, D., Mukhtarov, P., and Andonov, B.: Global structure, seasonal and interannual variability of the migrating semidiurnal tide seen in the SABER/TIMED temperatures (2002–2007), Ann. Geophys., 27, 687–703, doi:10.5194/angeo-27-687-2009, 2009.

Paulino, A. R., Batista, P. P., and Clemesha, R.: Lunar tides in the mesosphere and lower thermosphere over Cachoeira Paulista (22.7 degrees S; 45.0 degrees W), J. Atmos. Sol. Terr. Phys., 78–79, 31–36, doi:10.1016/j.jastp.2011.04.018, 2012.

Pedatella, N. M., Liu, H. L., and Hagan, M. E.: Day-to-day migrating and nonmigrating tidal variability due to the six-day planetary wave, J. Geophys. Res.-Space, 117, A06301, doi:10.1029/2012JA017581, 2012.

Portnyagin, Y. I., Forbes, J. M., Fraser, G. J., Vincent, R. A., Avery, S. K., Lysenko, I. A., and Makarov, N. A.: Dynamics of the Antarctic and Arctic mesosphere and lower thermosphere regions. 2. The Semidiurnal tide, J. Atmos. Terr. Phys., 55, 843–855, doi:10.1016/0021-9169(93)90025-T, 1993.

Riggin, D. M., Meyer, C. K., Fritts, D. C., Jarvis, M. J., Murayama, Y., Singer, W., Vincent, R. A., and Murphy, D. J.: MF radar observations of seasonal variability of semidiurnal motions in the mesosphere at high northern and southern latitudes, J. Atmos. Sol. Terr. Phys., 65, 483–493, doi:10.1016/S1364-6826(02)00340-1, 2003.

Sandford, D. J. and Mitchell, N. J.: Lunar tides in the Mesosphere over Ascension Island (8° S, 14.4° W), Ann. Geophys., 25, 9–12, doi:10.5194/angeo-25-9-2007, 2007.

Smith, A. K.: Global dynamics of the MLT, Surv. Geophys., 33, 1177–1230, doi:10.1007/s10712-012-9196-9, 2012.

Sridharan, S., Tsuda, T., and Gurubaran, S.: Long-term tendencies in the mesosphere/lower thermosphere mean winds and tides as observed by medium-frequency radar at Tirunelveli (8.7° N, 77.8° E), J. Geophys. Res.-Atmos., 115, D08109, doi:10.1029/2008JD011609, 2010.

Teitelbaum, H., Vial, F., Manson, A. H., Giraldez, R., and Massebeuf, M.: Non-linear interaction between the diurnal and semidiurnal tides – terdiurnal and diurnal secondary waves, J. Atmos. Terr. Phys., 51, 627–634, doi:10.1016/0021-9169(89)90061-5, 1989.

Tsuda, T., Ohnishi, K., Isoda, F., Nakamura, T., Vincent, R. A., Reid, I. M., Harijono, S. W. B., Sribimawati, T., Nuryanto, A., and Wiryosumarto, H.: Coordinated radar observations of atmospheric diurnal tides in equatorial regions, Earth Planets Space, 51, 579–592, 1999.

Vincent, R. A., Tsuda, T., and Kato, S.: A comparative study of mesospheric solar tides observed at Adelaide and Kyoto, J. Geophys. Res.-Atmos., 93, 699–708, doi:10.1029/JD093iD01p00699, 1988.

Vincent, R. A., Kovalam, S., Fritts, D. C., and Isler, J. R.: Long-term MF radar observations of solar tides in the low-latitude mesosphere: Interannual variability and comparisons with the GSWM, J. Geophys. Res-Atmos., 103, 8667–8683, 1998.

Ward, W. E., Oberheide, J., Goncharenko, L. P., Nakamura, T., Hoffmann, P., Singer, W., Chang, L. C., Du, J., Wang, D.-Y, Batista, P., Clemesha, B., Manson, A. H., Riggin, D. M., She, C.-Y., Tsuda, T., and Yuan, T.: On the consistency of model, ground-based and satellite observations of tidal signatures: Initial results from the CAWSES tidal campaigns, J. Geophys. Res., 115, D07107, doi:10.1029/2009JD012593, 2010.

Williams, C. R. and Avery, S. K.: Diurnal nonmigrating tidal oscillations forced by deep convective clouds, J. Geophys. Res.-Atmos, 101, 4079–4091, 1996.

Wu, Q., Ortland, D. A., Solomon, S. C., Skinner, W. R., and Niciejewski, R. J.: Global distribution, seasonal, and inter-annual variations of mesospheric semidiurnal tide observed by TIMED TIDI, J. Atmos. Sol. Terr. Phys., 73, 2482–2502, 2011.

Xu, J., Smith, A. K., Liu, H.-L., Yuan, W., Wu, Q., Jiang, G., Mlynczak, M. G., Russell III, J. M., and Franke, S. J.: Seasonal and quasi-biennial variations in the migrating diurnal tide observed by Thermosphere, Ionosphere, Mesosphere, Energetics and Dynamics (TIMED), J. Geophys. Res., 114, D13107, doi:10.1029/2008JD011298, 2009a.

Xu, J., Smith, A. K., Liu, H.-L., Yuan, W., Wu, Q., Jiang, G., Mlynczak, M. G., and Russell III, J. M.: Estimation of the equivalent Rayleigh friction in mesosphere/lower thermosphere region from the migrating diurnal tides observed by TIMED, J. Geophys. Res., 114, D23103, doi:10.1029/2009JD012209, 2009b.

Younger, P. T., Pancheva, D., Middleton, H. R., and Mitchell, N. J.: The 8-hour tide in the Arctic mesosphere and lower thermosphere, J. Geophys. Res.-Space, 107, 1420, doi:10.1029/2001JA005086, 2002.

Zhang, X., Forbes, J. M., and Hagan, M. E.: Longitudinal variation of tides in the MLT region: 1. Tides driven by tropospheric net radiative heating, J. Geophys. Res.-Atmos., 115, A06316, doi:10.1029/2009JA014897, 2010.